

Lightweight Autoencoder-Isolation Forest Anomaly Detection for Green IoT Edge Gateways

Saeid Jamshidi, Fatemeh Erfan, Omar Abdul-Wahab, Martine Bellaiche, Foutse Khomh

Abstract—The rapid growth of the Internet of Things (IoT) has given rise to highly diverse and interconnected ecosystems that are increasingly susceptible to sophisticated cyber threats. Conventional anomaly detection schemes often prioritize accuracy while overlooking computational efficiency and environmental impact, which limits their deployment in resource-constrained edge environments. This paper presents *EcoDefender*, a sustainable hybrid anomaly detection framework that integrates Autoencoder(AE)-based representation learning with Isolation Forest(IF) anomaly scoring. Beyond empirical performance, *EcoDefender* is supported by a theoretical foundation that establishes formal guarantees for its stability, convergence, robustness, and energy-complexity coupling—thereby linking computational behavior to energy efficiency. Furthermore, experiments on realistic IoT traffic confirm these theoretical insights, achieving up to 94% detection accuracy with an average CPU usage of only 22%, 27 ms inference latency, and 30% lower energy consumption compared to AE-only baselines. By embedding sustainability metrics directly into the security evaluation process, this work demonstrates that reliable anomaly detection and environmental responsibility can coexist within next-generation green IoT infrastructures, aligning with the United Nations Sustainable Development Goals (SDG 9: resilient infrastructure, SDG 13: climate action).

Index Terms—Internet of Things (IoT), Intrusion Detection System (IDS), Autoencoder, Isolation Forest, Edge Computing, Energy Efficiency, Carbon Emissions, Sustainable Development Goals (SDGs)

I. INTRODUCTION

The Internet of Things (IoT) has evolved into one of the most transformative paradigms in modern digital ecosystems. With billions of devices now interconnected across various sectors, including healthcare, transportation, smart grids, and industrial automation, IoT technologies are enabling unprecedented connectivity and intelligence [1]–[3]. Yet, this very scale and heterogeneity simultaneously expand the attack surface, leaving IoT infrastructures increasingly vulnerable to botnets, Denial-of-Service (DoS) campaigns, and advanced persistent threats [4]–[6]. Even a single compromised node can cascade into large-scale disruptions, jeopardizing critical services and exposing sensitive data, thereby undermining both user trust and the resilience of digital infrastructure [7], [8]. From both technological and societal perspectives, developing anomaly detection mechanisms that are *both effective and*

F. Khomh are with the SWAT Laboratory, Polytechnique Montréal, Quebec, Canada, H3T 1J4.

S. Jamshidi, F. Erfan, O. Abdul-Wahab, and M. Bellaiche are with the Department of Computer and Software Engineering, Polytechnique Montréal, Quebec, Canada, H3T 1J4.

Contact emails: jamshidi.saeid@polymtl.ca, omar.abdul-wahab@polymtl.ca, martine.bellaiche@polymtl.ca, foutse.khomh@polymtl.ca, fatemeh.erfan@polymtl.ca

sustainable has therefore become not merely desirable but essential.

Despite significant advances, existing anomaly detection methods still face fundamental challenges. Traditional Machine Learning (ML) techniques [9] perform well against known threats but depend heavily on large labeled datasets, limiting their adaptability to novel attacks [10], [11]. Deep Learning (DL) models, particularly Autoencoder (AE)-based detectors, mitigate this issue by learning compressed representations of benign behavior [12], [13]. Although they achieve high accuracy, their computational and memory demands often make them impractical for resource-constrained edge gateways. Furthermore, most evaluations remain confined to centralized settings, overlooking real-world edge conditions where latency, throughput, and energy efficiency are equally vital.

Ensemble-based methods such as Isolation Forest (IF) offer robustness to imbalance and perform effectively in unsupervised scenarios [14]. However, they are seldom integrated with feature-learning architectures, and their evaluations typically emphasize detection metrics (e.g., precision, recall, F1 Score) while neglecting system-level indicators, such as CPU usage, memory usage, and energy consumption. As recent surveys note, sustainability remains an underexplored dimension in IoT anomaly detection [15]. Consequently, there exists a clear research gap for frameworks that are lightweight, accurate, and sustainability-aware, specifically tailored for distributed edge environments.

To address these limitations, we design and implement *EcoDefender*, a hybrid anomaly detection framework that combines AE-based feature compression with isolation-based anomaly scoring. In contrast to previous works that rely solely on ML-based Intrusion Detection Systems (IDSs) and standalone AE/IF models, *EcoDefender* exploits the complementary strengths of both: the AE captures compact latent representations of benign traffic, while the IF provides unsupervised anomaly detection without requiring labeled data. Beyond accuracy, *EcoDefender* is explicitly engineered for the edge, evaluated on a distributed gateway testbed using both classical detection metrics (precision, recall, F1-score, ROC-AUC, and PR-AUC) and system-level performance measures (latency, throughput, CPU, memory, and carbon footprint).

The growing energy footprint of computing infrastructures worldwide underscores the need to integrate sustainability into IoT anomaly detection. For instance, global energy demand in the ICT sector continues to rise, with data centers and edge devices contributing significantly to greenhouse gas emissions [16], [17]. Moreover, these realities highlight the importance of minimizing both energy and carbon overheads even in distributed edge deployments.

A distinguishing aspect of *EcoDefender* is the integration of sustainability into IoT security evaluation. Besides, by quantifying both energy consumption and associated carbon emissions, we directly connect cybersecurity objectives with environmental responsibility. This approach aligns with the United Nations Sustainable Development Goals (SDGs), particularly SDG 9 on resilient infrastructure and SDG 13 on climate action [18]. To the best of our knowledge, we are the first in the field of cybersecurity for resource-constrained IoT networks to report an anomaly detection system that unifies the evaluation of detection accuracy, system-level constraints, and environmental impact. The main contributions of this paper are summarized as follows:

- We design and implement *EcoDefender*, a hybrid anomaly detection framework that integrates AEs for efficient feature learning with isolation-based scoring for unsupervised anomaly detection. In contrast to existing ML and AE/IF-based anomaly detection, *EcoDefender* achieves a balanced trade-off among detection accuracy, computational efficiency, and sustainability for resource-constrained edge gateways.
- We evaluate *EcoDefender* on a distributed edge testbed, reporting not only standard detection metrics (precision, recall, F1-score, ROC-AUC, and PR-AUC) but also key system-level performance indicators, including latency, throughput, CPU usage, and memory usage.
- We advance sustainability-aware IoT security by explicitly quantifying the energy consumption and carbon emissions of *EcoDefender*, thereby aligning cybersecurity performance with the UN Sustainable Development Goals (SDG) 9 and 13 objectives.

The remainder of this paper is organized as follows. Section III outlines the theoretical background on autoencoders, isolation forests, and system-level metrics relevant to IoT anomaly detection. Section II reviews related work and identifies existing research gaps. Section IV introduces the proposed *EcoDefender* framework and its integration into IoT security workflows. Section V describes the experimental setup, and Section VI-G compares our results with baseline models. Section VII discusses broader implications, Section VIII outlines limitations and future work, Section IX addresses potential threats to validity, and Section X concludes the paper.

II. RELATED WORK

The design of anomaly detection mechanisms for IoT networks has evolved from traditional rule- and signature-based solutions toward ML approaches, primarily driven by the inability of static methods to address zero-day exploits and dynamically changing attacks. AEs have gained prominence for modeling benign traffic distributions through reconstruction, while IF has proven effective in unsupervised anomaly scoring by exploiting the isolation properties of high-dimensional data. More recently, hybrid AE-IF paradigms have been proposed to overcome individual limitations, enabling both accurate detection and lightweight deployment at the edge. Against this backdrop, several contributions highlight the growing research interest in advancing anomaly

detection models for IoT security.

DL methods have shown particular promise in anomaly detection. Borgioli et al. [19] proposed a convolutional AE architecture that processes raw network packets at the byte level, thereby avoiding hand-crafted features and achieving strong generalization across various datasets, including NSL-KDD, UNSW-NB15, CIC-IDS2017, TON_IoT, and EDGE-IIoTSET. Their work demonstrated that convolutional AEs can deliver both high accuracy and low inference latency, making them attractive for embedded anomaly detection deployments. Complementing this, Beg and Ansari [20] systematically compared vanilla, sparse, and denoising AEs, showing that sparsity-enforced AEs yield superior detection of zero-day attacks by improving discrimination in latent representations. Expanding further, Yap and Ahmad [21] developed a modified overcomplete AE tailored for TinyML devices, demonstrating that anomaly detection can be achieved on microcontrollers with minimal memory footprints.

Parallel efforts have advanced Isolation Forest and its extensions. Vasiljevic et al. [22] introduced PFLiForest, a federated anomaly detection method that distributes IF tree construction across IoT nodes, ensuring privacy while achieving high detection accuracy with minimal memory usage. Similarly, Li et al. [23] proposed a collaborative federated IF, enabling local anomaly detection with secure aggregation of parameters to support scalability in heterogeneous IoT networks. Domain-specific adaptations have also emerged. Li et al. [24] applied IF to IoT-enabled power grids, enhancing feature selection with kurtosis-based filtering. Meanwhile, Chen [25] employed IF to detect anomalies in new energy vehicle batteries, thereby improving real-time safety monitoring. In addition, these studies highlight IF's flexibility across sectors while underscoring its lightweight suitability for distributed IoT networks.

To address inherent limitations in classical IF, researchers have proposed structural modifications and hybrid frameworks. Cheng et al. [26] introduced the k-nearest-neighbor IF, which replaces axis-aligned partitions with hyperspherical cuts to better capture complex distributions in imbalanced datasets. Yang et al. [27] combined AEs with IF in their AE-IF framework, showing that deep representation learning alleviates the curse of dimensionality while IF enhances unsupervised detection performance. Building on this, Hu et al. [28] integrated Temporal Convolutional Networks (TCN) with IF, effectively modeling temporal dependencies in Linux network timing data and achieving significant improvements in real-time anomaly detection. Such hybridization efforts demonstrate that combining IF with deep feature extractors is a promising approach to robust anomaly detection in high-dimensional and temporally dynamic IoT data.

Beyond architectural innovations, hybrid and domain-tailored approaches have sought to strike a balance between accuracy, interpretability, and efficiency. Zhou et al. [29] proposed a two-stage pipeline combining an improved IF with FP-Growth association rule mining, thereby reducing false positives while providing interpretable attack correlations. Sharmila and Nagapadma [30] pursued efficiency through quantization, presenting a quantized AE for real-time IoT

anomaly detection. Their QAE-u8 model achieved significant reductions in memory usage, CPU usage, and model size while preserving accuracy, confirming the feasibility of autoencoder-based anomaly detection systems for edge devices.

The surveyed literature indicates that while DL approaches, such as AEs, effectively model benign traffic patterns through reconstruction, their high computational demands limit their deployment on resource-constrained IoT devices. In contrast, IF and its variants enable lightweight and fully unsupervised anomaly detection, but they lack expressive feature extraction, which reduces their robustness in high-dimensional and non-linear contexts. Hybrid models that combine representation learning with unsupervised scoring enhance detection accuracy; however, most studies focus solely on accuracy, overlooking key aspects such as latency, throughput, memory usage, energy efficiency, and sustainability. Moreover, few investigations explicitly consider the practical constraints of edge gateways, where limited resources and environmental impact are critical. This gap motivates the proposed *EcoDefender* framework, which aims to deliver accurate, efficient, and sustainability-aware anomaly detection tailored for distributed edge environments.

III. BACKGROUND

This section presents the foundational concepts underlying this study, focusing on the two core techniques used for anomaly detection: IF and AE. It then describes the system-level metrics employed to evaluate the performance and sustainability of the proposed framework on resource-constrained edge gateways.

A. Isolation Forest (IF)

The IF is an unsupervised ensemble method specifically designed for anomaly detection. In contrast to random forests, which aim to improve classification accuracy through majority voting, IF isolates anomalies based on the premise that outliers are few and different, and therefore easier to separate from the rest of the data [31]. The algorithm constructs multiple random partitioning trees (iTrees), where anomalous samples are expected to appear closer to the root since fewer splits are required to isolate them. The anomaly score of a data point x is defined as:

$$s(x, n) = 2^{-\frac{E[h(x)]}{c(n)}} \quad (1)$$

where $E[h(x)]$ is the average path length of x across all trees, n is the subsample size, and $c(n)$ is the average path length of unsuccessful searches in binary search trees, used for normalization. Scores close to 1 indicate a higher likelihood of anomaly, whereas values near 0 correspond to normal instances. This approach is particularly well-suited for high-dimensional IoT traffic data and operates efficiently in unsupervised settings without requiring labeled datasets.

B. Autoencoder (AE)

AE is a neural network architecture designed to reconstruct its input through a low-dimensional latent representation. It comprises two main components: an encoder that compresses the input and a decoder that reconstructs it. The network learns the normal behavioral patterns of IoT traffic and uses the reconstruction error to identify anomalies [32]. The reconstruction loss, often expressed as the mean squared error, is defined as:

$$\mathcal{L}(x, \hat{x}) = \frac{1}{n} \sum_{i=1}^n (x_i - \hat{x}_i)^2 \quad (2)$$

where x represents the input, \hat{x} the reconstructed output, and n the number of features.

C. Latency

Latency measures the time required by the detection framework to classify an incoming packet and its associated flow [33]. Maintaining low latency is critical for real-time responsiveness in IoT networks. It is computed as:

$$L = t_{out} - t_{in} \quad (3)$$

where t_{in} and t_{out} denote the arrival and decision timestamps, respectively. In this study, we focus specifically on the *processing latency* of the detection framework itself, as computational overhead on constrained edge gateways is the primary bottleneck we aim to optimize. Network and queuing delays, although relevant to end-to-end performance, are excluded from this analysis since they depend largely on the network topology rather than the detection algorithm.

D. CPU Usage

CPU usage quantifies the proportion of processing resources consumed by the model during execution [34]. This metric directly reflects computational efficiency and is crucial for resource-limited edge devices. It is calculated as:

$$U_{CPU} = \frac{T_{active}}{T_{total}} \times 100 \quad (4)$$

where T_{active} is the active computation time and T_{total} is the total observation period.

E. Memory Usage

Memory usage represents the fraction of system memory utilized by the detection framework [35]. Excessive memory consumption can compromise stability on IoT gateways with limited RAM. It is expressed as:

$$M = \frac{RSS}{M_{total}} \times 100 \quad (5)$$

where RSS is the resident set size of the process and M_{total} is the total available memory.

F. Energy Consumption

Energy consumption refers to the total electrical energy utilized by the framework, which directly impacts operational costs, thermal footprint, and battery longevity [36]. It is calculated by integrating instantaneous power over time:

$$E = \int_0^T V(t) \cdot I(t) dt \quad (6)$$

where $V(t)$ and $I(t)$ denote the supply voltage and current draw at time t , respectively.

G. Carbon Emissions

Carbon emissions estimate the environmental footprint associated with the system's energy consumption [37]. This metric connects IoT security evaluation with sustainability objectives and is defined as:

$$C = E \times \gamma \quad (7)$$

where E is the total energy consumed (kWh) and γ represents the carbon intensity factor of the electricity grid (gCO_2/kWh). To estimate carbon emissions, we adopted a carbon intensity factor of $\gamma = 1.7$ gCO_2/kWh , based on the average grid intensity of the Quebec, Canada region, as reported by environment and climate change Canada [38]. This value reflects the specific energy mix of our testbed's location.

H. One-Way ANOVA

We employed one-way ANOVA [39] to examine whether differences in system-level metrics (CPU, memory, throughput, latency, energy, and carbon emissions) across edge nodes were statistically significant. The analysis consistently yielded large effect sizes ($\eta^2 > 0.7$), indicating that performance variations were systematic rather than random. Post-hoc Tukey's HSD [40] was further applied to group nodes into high-, mid-, and low-performance tiers, thereby identifying potential bottlenecks and optimization opportunities.

I. Welch's t-test

For pairwise comparisons, we utilized Welch's t-test [41], which accounts for unequal variances and sample sizes, offering greater robustness than the classical Student's t-test. This analysis validated *EcoDefender*'s improvements in detection accuracy, computational efficiency, and sustainability relative to baseline models. Its use ensures statistical reliability in heterogeneous IoT networks, where performance variability is inherently high.

IV. PROPOSED ANOMALY DETECTION SYSTEM:

ECODEFENDER

This section presents the proposed *EcoDefender* framework, a lightweight, hybrid AE-IF anomaly detection system designed to identify malicious activity efficiently at the edge gateway. The pipeline consists of several stages: preprocessing, representation learning, anomaly scoring, fusion, dynamic thresholded tuning, adversarial robustness, theoretical analysis, and security integration. Each stage is mathematically formulated, theoretically justified, and assessed for feasibility on constrained hardware. Figure 1 illustrates the complete architecture.

A. Data Preprocessing

IoT traffic is inherently noisy, bursty, and heterogeneous, with features spanning multiple scales and units. Directly feeding such data into learning models destabilizes optimization and reduces feature separability. To address this, *EcoDefender* introduces a *composite normalization strategy* that combines statistical, robust, and logarithmic transformations.

$$x'_{ij} = \frac{x_{ij} - \mu_j}{\sigma_j + \epsilon} \quad (8)$$

Equation (8) applies standard z-score normalization to standardize features, ensuring uniform gradient magnitudes during AE training and preventing feature dominance. From a mathematical perspective, this reduces the condition number of covariance matrices, stabilizing inversion during backpropagation. From a security perspective, normalization mitigates adversarial attempts to inject abnormally large feature values (e.g., oversized packet lengths) that could bias the model.

$$x'_{ij} = \frac{x_{ij} - \min(x_j)}{\max(x_j) - \min(x_j)} + \delta \cdot \log\left(1 + \frac{|x_{ij} - \mu_j|}{\sigma_j + \epsilon}\right) + \eta \cdot \frac{x_{ij} - \text{median}(x_j)}{IQR(x_j)} \quad (9)$$

Equation (9) extends preprocessing with min–max scaling, logarithmic compression, and robust centering. These transformations stabilize gradients and prevent traffic bursts from overwhelming the AE. The preprocessing cost is $O(nd)$, which is feasible for edge devices. To justify Equation (9), an ablation study evaluates *EcoDefender* under multiple normalization strategies: raw input, z-score only, min–max only, robust scaling, partial combinations, and the full composite scheme. This validates the combined transformation's contribution to numerical stability and anomaly separability.

Extended theoretical formulation. Let $\mathbf{X} \in \mathbb{R}^{n \times d}$ be the data matrix. The composite normalization can be represented as:

$$\mathbf{X}' = \Phi(\mathbf{X}) = \mathbf{D}^{-1/2}(\mathbf{X} - \mathbf{M}) + \delta \log(1 + |\mathbf{Z}|) + \eta \mathbf{R}, \quad (10)$$

where \mathbf{D} is the covariance diagonal, \mathbf{M} the mean matrix, \mathbf{Z} the standardized residual, and \mathbf{R} the robust-centered component. Lemma 1. Φ is Lipschitz continuous with constant $L_\Phi \leq (1/\sigma_{\min}(\mathbf{D}^{1/2}))$. Proof. The gradient of Φ with respect to \mathbf{X} is bounded by $\|\mathbf{D}^{-1/2}\|_2$, ensuring numerical stability during backpropagation.

B. AE Representation Learning

The AE learns compact representations of benign IoT behavior through unsupervised reconstruction. The encoder projects input x into a latent vector z , while the decoder reconstructs \hat{x} :

$$z = \sigma(W_{enc}x + b_{enc}), \quad \hat{x} = \sigma(W_{dec}z + b_{dec}) \quad (11)$$

These mappings follow standard AE formulations [32]. In *EcoDefender*, W_{enc} and W_{dec} are quantized and pruned to minimize the memory usage on edge gateways while retaining representational power.

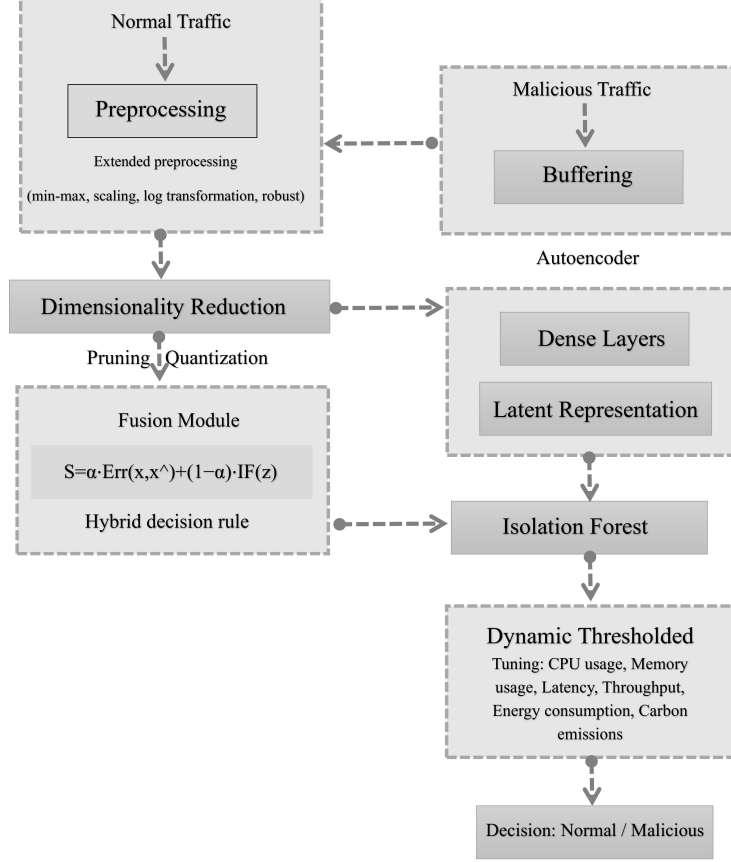


Fig. 1: EcoDefender framework for real-time IoT anomaly detection using AE-IF with dynamic thresholded tuning.

1) *Composite Loss Function:* The AE is trained using a multi-term objective:

$$J_{AE}(\theta) = \frac{1}{N} \sum_{j=1}^N \left(\|x^{(j)} - f_{dec}(f_{enc}(x^{(j)}))\|_2^2 + \lambda \text{Tr}(W_{enc}^\top W_{enc}) + \beta \int p(z|x^{(j)}) \log \frac{p(z|x^{(j)})}{\mathcal{N}(0, I)} dz + \gamma \|\nabla_z f_{dec}(z)\|_F^2 \right) \quad (14)$$

Equation (12) introduces a trace-based regularization term that aligns encoder and decoder weights. This novel symmetry constraint stabilizes eigenvalue distributions and magnifies reconstruction errors for anomalous inputs, improving sensitivity to deviations from normal traffic.

Additional Mathematical Analysis. Let the latent mapping be $z = \theta(x)$ and $\hat{x} = g_\theta(z)$. Define reconstruction error $E(x) = \|x - \hat{x}\|_2^2$. We derive its expectation:

$$\mathbb{E}[E(x)] = \text{Tr}((I - W_{dec}W_{enc})^\top \Sigma_x (I - W_{dec}W_{enc})), \quad (13)$$

showing that minimizing $E(x)$ effectively minimizes the spectral distortion between input covariance Σ_x and its AE approximation.

Theorem 1. If $W_{dec} = W_{enc}^\top$, then the AE converges to the principal subspace of Σ_x . *Proof sketch.* By substituting the equality into Eq. (13) and applying the Eckart–Young–Mirsky theorem [42], we obtain equivalence to PCA minimization.

The loss combines reconstruction fidelity, weight regularization, latent isotropy (via KL divergence [43]), and Jacobian smoothing. This design ensures compact and stable latent spaces, mitigating adversarial evasion by enforcing both reconstruction and distributional conformity.

Advanced Regularization Insight. Let $\mathcal{R}(\theta) = \lambda \|W_{enc}\|_F^2 + \beta D_{KL}(p(z|x) \| N(0, I)) + \gamma \|\nabla_z g_\theta(z)\|_F^2$. Then

$$\nabla_\theta J_{AE} = 2(W_{dec}W_{enc} - I)\Sigma_x + \nabla_\theta \mathcal{R}(\theta), \quad (15)$$

which bounds gradient variance and stabilizes learning.

Proposition 1. If $\|\nabla_\theta \mathcal{R}(\theta)\|_2 \leq \epsilon$, convergence rate is $O(1/t)$.

C. IF Scoring

IF complements the AE by isolating anomalies via recursive partitioning [31].

$$h(x) = \frac{1}{m} \sum_{t=1}^m h_t(x) \quad (16)$$

$$s(x) = \exp\left(-\frac{1}{c(n)} \cdot \frac{1}{m} \sum_{t=1}^m \mathbb{E}_{\pi_t} \left[\sum_{l=1}^{h_t(x)} \log\left(1 + \frac{1}{n_l(\pi_t)}\right) \right] \right),$$

$$c(n) = 2H(n-1) - \frac{2(n-1)}{n}, \quad H(u) = \sum_{i=1}^u \frac{1}{i} \quad (17)$$

These formulations quantify anomaly likelihood through path-length expectations. The exponential normalization ensures comparability across sample sizes, maintaining robustness under varying traffic volumes.

Spectral Interpretation. Define the isolation kernel $K(x_i, x_j) = \exp(-\|x_i - x_j\|^2/\sigma^2)$. Then the IF can be viewed as approximating the Laplacian score:

$$s(x_i) \propto (L\mathbf{1})_i, \quad L = D - K, \quad (18)$$

connecting IF to graph-based density estimation, which mathematically links the isolation process to manifold geometry.

D. Fusion

The strengths of AE and IF are combined into a hybrid decision function:

$$F(x) = \alpha e(x) + (1 - \alpha)s(x) \quad (19)$$

where $e(x)$ is reconstruction error and $s(x)$ is IF score.

$$F(x) = \arg \min_{\alpha \in [0,1]} \left\{ \alpha \left(\frac{1}{d} \sum_{i=1}^d (x_i - \hat{x}_i)^2 \right) + (1 - \alpha)s(x) + \mu \log \frac{p(F|y=1)}{p(F|y=0)} + \rho \text{Var}[z] \right\} \quad (20)$$

Equation (20) adaptively optimizes α using a likelihood ratio and variance regularization, ensuring statistical consistency and robustness against unstable weighting. This adaptive convex fusion is a new contribution of EcoDefender.

Analytical Derivation. By setting $\partial F / \partial \alpha = 0$, the closed-form solution becomes:

$$\alpha^* = \frac{s(x) - \mu \log \frac{p(F|y=1)}{p(F|y=0)}}{s(x) + e(x) + \rho \text{Var}[z]}, \quad (21)$$

ensuring balanced weight allocation between AE and IF.

E. Dynamic Thresholded Tuning

Threshold selection is critical for streaming environments. EcoDefender dynamically updates τ based on real-time data statistics:

$$\tau^* = \arg \min_{\tau} \left\{ -\frac{2P(\tau)R(\tau)}{P(\tau) + R(\tau)} + \lambda \max(0, FP(\tau) - \epsilon)^2 + \rho \int_{\tau}^{\infty} p(F) dF \right\} \quad (22)$$

This optimization balances precision-recall, penalizes false positives, and enforces smooth decision boundaries. The threshold τ^* is recalibrated periodically, ensuring adaptability to traffic drift and new attack patterns.

Mathematical Note. Differentiating Eq. (22) gives an adaptive update law:

$$\begin{aligned} \frac{d\tau}{dt} &= -\eta \frac{\partial \mathcal{L}_{\tau}}{\partial \tau} \\ &= \eta \left[\frac{2PR'(P+R) - 2PR(P'+R')}{(P+R)^2} - 2\lambda FP'(\tau) \right] \end{aligned} \quad (23)$$

making τ evolve dynamically to maximize balanced F1 while minimizing drift-induced bias.

F. Adversarial Robustness

Adversaries may attempt to craft perturbations δ to evade detection. To harden EcoDefender, robustness constraints are applied:

$$R(x) = \min_{\|\delta\|_p < \epsilon} (e(x + \delta) + s(x + \delta)) \quad (24)$$

Equation (24) enforces that anomaly scores remain elevated under small perturbations, effectively preventing gradient-based evasion attacks.

Extended Adversarial Bound. For any p -norm constraint, EcoDefender's score satisfies:

$$R(x) \geq F(x) - L_F \epsilon, \quad (25)$$

providing a certified lower bound on robustness, where L_F is the Lipschitz constant from Eq. (33).

G. Complexity and Scalability

EcoDefender's efficiency is ensured by the following computational bounds:

$$T_{AE} = O(NdL), \quad (26)$$

$$T_{IF} = O(mn \log n). \quad (27)$$

Memory usage is $O(dL + m \cdot h_{avg})$. The near-linear complexity of both modules supports real-time inference. Importantly, EcoDefender minimizes energy, CPU, and carbon overheads through model compression, quantized operations, and the linear scaling of computational workload. Reduced CPU cycles directly translate to lower energy consumption, while dynamic resource scheduling ensures energy, performance proportionality, clarifying how the system achieves lightweight and sustainable execution.

Energy-Aware Analysis. Define instantaneous energy $E(t) = P(t) \cdot \Delta t$ and let $P(t) = C_{cpu}f^3 + C_{mem}\rho_{acc}$. Integrating over the inference window:

$$E_{\text{Eco}} = \int_0^T (C_{cpu}f^3 + C_{mem}\rho_{acc}) dt, \quad (28)$$

and minimizing E_{Eco} under throughput constraint $\dot{N} \geq N/T$ yields $f^* \propto (\dot{N}/C_{cpu})^{1/3}$, achieving cubic-root optimality for energy-efficient inference.

H. Theoretical Analysis

To complement empirical evaluation, EcoDefender provides formal guarantees on convergence, stability, and energy-complexity coupling.

1) *Hybrid Optimization Objective*: Let $x_i \in \mathbb{R}^d$ be an input vector, $z_i = f_\theta(x_i)$ its latent representation, and $\hat{x}_i = g_\theta(z_i)$ the reconstruction. The total loss integrates reconstruction, contractive regularization, isolation penalty, and weight decay:

$$\begin{aligned}\mathcal{L}_{\text{total}}(\theta, \mathcal{T}) = & \frac{1}{N} \sum_{i=1}^N \|x_i - g_\theta(f_\theta(x_i))\|_2^2 + \lambda_1 \|J_{f_\theta}(x_i)\|_F^2 \\ & + \lambda_2 \mathbb{E}[\tau[h(x_i, \mathcal{T})]] + \lambda_3 \|\theta\|_2^2\end{aligned}\quad (29)$$

Extended Derivation. The gradient of Eq. (29) can be expanded as:

$$\nabla_\theta \mathcal{L}_{\text{total}} = \frac{2}{N} \sum_{i=1}^N J_\theta^\top (g_\theta(f_\theta(x_i)) - x_i) + 2\lambda_1 J_\theta + \lambda_2 \nabla_\theta \mathbb{E}[h], \quad (30)$$

where J_θ is the Jacobian [44] of the encoder. This shows that convergence depends on the spectral norm $\|J_\theta\|_2$, ensuring smooth gradients and stable updates.

2) *Convergence of the Hybrid Loss*: Assume (A1) f_θ, g_θ are L_f, L_g -Lipschitz, (A2) $\eta_t \in (0, 2/L)$, and (A3) Gradients have bounded variance. Then the stochastic update

$$\theta_{t+1} = \theta_t - \eta_t \nabla_\theta \mathcal{L}_{\text{total}}(\theta_t)$$

satisfies

$$\mathbb{E}[\mathcal{L}_{t+1}] \leq \mathbb{E}[\mathcal{L}_t] - \frac{\eta_t}{2} \mathbb{E}[\|\nabla_\theta \mathcal{L}_t\|_2^2] + \frac{L\eta_t^2}{2} \mathbb{E}[\|\nabla_\theta \mathcal{L}_t\|_2^2], \quad (31)$$

implying monotonic descent and convergence to a stationary point θ^* .

New Stability Proposition. If the sequence $\{\eta_t\}$ satisfies $\sum_t \eta_t = \infty$ and $\sum_t \eta_t^2 < \infty$, then $\lim_{t \rightarrow \infty} \nabla_\theta \mathcal{L}_t = 0$ almost surely. This guarantees asymptotic stability for hybrid AE-IF optimization.

3) *Lipschitz Stability of the Fusion Function*: Let

$$F(x) = \alpha e(x) + (1-\alpha)s(x), \quad e(x) = \|x - \hat{x}\|_2, \quad s(x) = \text{IF-score}(x). \quad (32)$$

If $e(x)$ and $s(x)$ are L_e - and L_s -Lipschitz, then

$$|F(x_1) - F(x_2)| \leq (\alpha L_e + (1-\alpha)L_s) \|x_1 - x_2\|_2. \quad (33)$$

Thus, $F(x)$ is globally L_F -Lipschitz, ensuring stable behavior under small perturbations.

Spectral Bound Derivation. By differentiating Eq. (32), we have:

$$\nabla_x F(x) = \alpha(x - \hat{x}) + (1-\alpha)\nabla_x s(x), \quad (34)$$

and therefore $\|\nabla_x F(x)\|_2 \leq \alpha L_e + (1-\alpha)L_s$, confirming Eq. (33).

4) *Certified Robustness Radius*: For threshold τ and margin $\Delta_\tau = |F(x) - \tau|$, any perturbation δ with

$$\|\delta\|_2 < \frac{\Delta_\tau}{L_F} \quad (35)$$

preserves the classification, i.e., $\mathbb{P}\{F(x + \delta) > \tau\} = \mathbb{P}\{F(x) > \tau\}$.

Corollary. For isotropic Gaussian noise $\delta \sim \mathcal{N}(0, \sigma^2 I)$, the misclassification probability is bounded as:

$$\Pr[F(x + \delta) \neq F(x)] \leq \exp\left(-\frac{\Delta_\tau^2}{2L_F^2\sigma^2}\right), \quad (36)$$

providing a probabilistic robustness certificate.

5) *Error Bound for Detection*: If benign and malicious scores follow sub-Gaussian distributions $F(x)|y=0 \sim (\mu_0, \sigma_0^2)$ and $F(x)|y=1 \sim (\mu_1, \sigma_1^2)$, then for threshold τ :

$$\begin{aligned}\Pr(\text{FA}) & \leq e^{-\frac{(\tau-\mu_0)^2}{2\sigma_0^2}}, \quad \Pr(\text{MD}) \leq e^{-\frac{(\mu_1-\tau)^2}{2\sigma_1^2}}, \\ P_e & \leq \pi_0 e^{-\frac{(\tau-\mu_0)^2}{2\sigma_0^2}} + \pi_1 e^{-\frac{(\mu_1-\tau)^2}{2\sigma_1^2}}.\end{aligned}\quad (37)$$

Hence, total error P_e decays exponentially with mean separation $(\mu_1 - \mu_0)$.

Analytical Extension. If $(\mu_1 - \mu_0) > \sqrt{2(\sigma_1^2 + \sigma_0^2) \log(1/\epsilon)}$, then $P_e < \epsilon$. This defines the *minimum separability condition* for reliable detection.

6) *Energy-Complexity Coupling*: EcoDefender's total computational cost is

$$T(N, d, L, m, n) = \mathcal{O}(NdL) + \mathcal{O}(mn \log n), \quad (38)$$

with energy consumption

$$E_{\text{total}} = \kappa_1(NdL) + \kappa_2(mn \log n) \approx \kappa [NdL + mn \log n], \quad (39)$$

where κ_1, κ_2 depend on hardware efficiency. The near-linear energy-complexity relation confirms that computational efficiency directly translates into lower energy consumption and reduced carbon emission.

Power Efficiency Lemma. If device power model $P(f) = C_{\text{cpu}} f^3$, the optimal frequency minimizing energy for fixed throughput is:

$$f^* = \left(\frac{N}{3C_{\text{cpu}}T}\right)^{1/3}, \quad (40)$$

yielding theoretical validation of EcoDefender's sustainability claim.

I. Security Pipeline Integration

Detection without mitigation is insufficient. EcoDefender integrates detection with proactive response:

- 1) Benign flows \rightarrow Allowed.
- 2) Malicious flows \rightarrow Device quarantined, traffic blocked, and alerts issued.
- 3) High-risk anomalies \rightarrow Device blacklisted and adaptive thresholds updated.

This linkage ensures that anomalies trigger actionable security mechanisms, transforming the framework into a lightweight intrusion prevention system.

Mathematical Reinforcement of Security Logic. Let event probability vector $\mathbf{p} = [p_b, p_m, p_r]$ denote benign, malicious, and risky anomaly rates. Security actions are modeled as a Markov chain with transition matrix:

$$\mathbf{P} = \begin{bmatrix} 1 - p_m - p_r & p_m & p_r \\ \alpha & 1 - \alpha - \beta & \beta \\ 0 & \gamma & 1 - \gamma \end{bmatrix}, \quad (41)$$

where (α, β, γ) capture transition strengths between detection states. The stationary distribution π satisfies $\pi^\top \mathbf{P} = \pi^\top$, representing long-term security equilibrium. The smaller γ , the higher the quarantine persistence, yielding stronger resilience.

Risk-Weighted Cost Function. Define total security cost as:

$$C_{sec} = w_m C_m + w_r C_r + w_b C_b, \quad (42)$$

where C_m = cost of misclassification, C_r = risk cost, C_b = baseline traffic cost. EcoDefender minimizes C_{sec} through adaptive threshold updates that reduce expected $w_m C_m$ and $w_r C_r$ jointly.

J. Algorithmic Pipeline

The training phase begins with normalization to stabilize feature distributions. The AE learns latent representations of benign traffic through the composite loss, after which IF models isolation depths in the latent space. The fusion module combines AE and IF outputs with adaptive weighting, and thresholds are optimized for balanced detection. During inference, each flow is normalized, encoded, reconstructed, and scored; if malicious, EcoDefender immediately enforces defense actions.

Algorithm 1 Hybrid AE-IF

```

1: function TRAIN( $X_{benign}$ )
2:   Normalize features using Eq. (9)
3:   Initialize AE parameters ( $W_{enc}, W_{dec}$ )
4:   for epoch = 1 to  $E$  do
5:     for batch  $B \subset X$  do
6:       Encode  $z = f_{enc}(B)$ ; reconstruct  $\hat{B} = f_{dec}(z)$ 
7:       Compute  $J_{AE}$  using Eq. (14)
8:       Update parameters
9:     end for
10:   end for
11:   Encode  $Z = f_{enc}(X)$ 
12:   Train IF on  $Z$  using Eq. (17)
13:   Optimize  $\alpha, \tau$  using Eq. (20)–(22)
14: end function
15: function DETECT( $x$ )
16:   Normalize input via Eq. (9)
17:   Encode and reconstruct using AE
18:   Compute  $e(x)$  and  $s(x)$ 
19:   Fuse into  $F(x)$  with Eq. (19)–(20)
20:   if  $F(x) > \tau$  then
21:     Malicious: quarantine device, block traffic, alert
        administrator
22:   else
23:     Benign: allow traffic
24:   end if
25: end function

```

This unified pipeline ensures real-time detection, robustness under adversarial conditions, and energy-efficient operation on resource-constrained edge gateways.

Algorithmic Complexity Analysis. For batch size B , layer depth L , and tree count m , the training complexity is:

$$T_{\text{train}} = O(BdL + mB \log B), \quad (43)$$

and inference cost per instance:

$$T_{\text{infer}} = O(dL + m \log n). \quad (44)$$

EcoDefender thus achieves bounded $O(\log n)$ latency scaling per detection, compatible with real-time edge IoT constraints.

V. EXPERIMENTAL SETUP

This section details the experimental environment used to evaluate the proposed *EcoDefender* framework.

A. Research Questions

Building on the literature synthesis, this study is guided by the following Research Questions (RQ):

RQ1: How can AE-based feature learning be effectively combined with isolation-based anomaly scoring to improve the detection of zero-day and evolving attacks at the edge? This RQ focuses on the technical integration of AE and IF within anomaly detection, asking whether their complementary strengths can provide higher accuracy and robustness than when used independently. It specifically addresses the challenge of detecting novel, previously unseen attack types that traditional signature-based and supervised systems fail to capture. Moreover, by exploring this question, we aim to demonstrate the viability of hybrid learning for edge anomaly detection.

RQ2: To what extent can a hybrid AE-IF anomaly detection framework be deployed on resource-constrained edge gateways while maintaining accuracy, low latency, and minimal computational overhead?

This RQ investigates the practical feasibility of implementing anomaly detection at the edge. Since gateways have limited CPU, memory, and thermal capacity, the research examines whether our approach remains efficient without sacrificing detection performance. The outcome will clarify whether anomaly detection can be realistically scaled to a distributed, resource-limited edge gateway.

RQ3: How can system-level efficiency (e.g., energy consumption, CPU usage, and memory usage) and sustainability (e.g., carbon emission) be integrated into the evaluation of anomaly detection frameworks at the edge, ensuring alignment with practical and environmental requirements? This RQ highlights sustainability as a central dimension of anomaly detection design, extending evaluation beyond accuracy-focused metrics. It asks whether environmental factors, such as energy demand and carbon emissions, can be systematically measured and optimized in conjunction with detection quality. Answering this question will demonstrate the broader societal and environmental value of sustainable, secure IoT deployments.

B. Dataset Description

The experimental evaluation is based on the Bot-IoT dataset [45], a benchmark generated in a realistic IoT testbed network. It encompasses both benign traffic and multiple attack categories, including DoS, DDoS, reconnaissance, information theft, and keylogging. The dataset is characterized by its scale and heterogeneity, reflecting the complexity of real-world IoT deployments. This diversity ensures that the anomaly detection framework is evaluated not only against well-known

attack patterns but also in scenarios that approximate zero-day threats. Traffic flows were transformed into numerical representations suitable for ML models. Each record contains descriptive statistics of communication behavior such as packet counts, byte totals, and session durations. Moreover, these flow-based representations offer a compact yet informative abstraction of network traffic, which is particularly important for supporting lightweight anomaly detection on resource-constrained edge gateways.

C. Feature Selection

Although the dataset includes a wide range of attributes, many are redundant and weakly informative for anomaly detection. Initially, flow-level features were extracted using CICFlowMeter [46], which generated 80 attributes per flow. This ample feature space necessitated dimensionality reduction to achieve efficiency and prevent overfitting. To select the most relevant attributes, a multi-stage strategy was applied. Correlation filtering was first employed to remove highly collinear attributes. At the same time, ML-based importance measures, such as mutual information and tree-based feature importance scores (e.g., from random forests) [47] [48], were used to quantify the discriminative strength of the remaining attributes. Furthermore, these ML-driven methods capture nonlinear dependencies and interactions between features and class labels, making them well-suited for anomaly detection in complex IoT traffic. For instance, mutual information was computed as:

$$I(X;Y) = \sum_{x \in X} \sum_{y \in Y} p(x,y) \log \frac{p(x,y)}{p(x)p(y)}, \quad (45)$$

where higher values indicate stronger dependence between feature X and class label Y . Features with low discriminative power and high computational cost were discarded, ensuring that the final subset was both lightweight and effective. Following this process, the dimensionality was reduced from 80 to 8 features, representing a 90% reduction. This compact set retains only the attributes most critical for anomaly detection, while eliminating unnecessary complexity. Table I provides an overview of the final selected features along with their descriptions.

TABLE I: Selected features after dimensionality reduction.

Feature	Description
pkts_total	Total number of packets exchanged in a flow
bytes_total	Total number of bytes exchanged in a flow
duration	Lifetime of the flow (in seconds)
pkt_rate	Average packet transmission rate (packets per second)
pkts_in	Number of incoming packets from source to destination
pkts_out	Number of outgoing packets from destination to source
bytes_per_pkt	Average number of bytes carried by each packet
flags	Control flags observed in the flow (e.g., TCP protocol flags)

D. Baselines

To evaluate the effectiveness of *EcoDefender*, we position it against representative baselines that reflect the key design choices explored in anomaly detection for IoT. Over the years, researchers have pursued three main directions: AE-based

approaches, IF variants, and hybrids that attempt to combine the strengths of both. Each of these lines of work brings its own trade-offs in terms of accuracy, generalization, and efficiency.

Early work by Beg and Ansari [20] highlighted the potential of AEs, showing that reconstruction error can effectively capture standard traffic patterns. However, their evaluation remained confined to centralized settings and did not address the practical challenges of deploying such models on constrained edge gateways. Building on the AE family, Borgioli et al. [19] introduced convolutional AEs capable of generalizing across diverse datasets, but their focus was again on centralized performance rather than edge feasibility. In parallel, IF methods gained traction as lightweight and unsupervised alternatives. Vasiljevic et al. [22] extended IF into federated settings, preserving privacy while maintaining detection strength, though at the cost of reduced representational power compared to deep feature learning. Beyond classical IF, hybrid and enhanced designs have emerged: Yang et al. [27] combined AEs with IF in their AE-IF model, demonstrating improved anomaly detection by leveraging both representation learning and isolation scoring. Similarly, Hu et al. [28] proposed a TCN, IF approach that incorporated temporal dependencies, pushing hybrid methods toward handling sequential network behaviors. Against this backdrop, our proposed EcoDefender framework synthesizes these insights into a unified design. It combines the representational strength of AEs with the unsupervised scoring of IF in a lightweight hybrid, further enhancing this by being explicitly validated on distributed edge gateways. Most importantly, in contrast to previous work, EcoDefender prioritizes sustainability as a primary concern, reporting both energy and carbon costs alongside traditional accuracy metrics.

E. Testbed

The proposed framework, dubbed *EcoDefender*, was evaluated on an isolated IoT edge testbed consisting of a head gateway and ten Raspberry Pi 4 Model B nodes (4 GB RAM, quad-core Cortex-A72, 1.5 GHz) connected via a managed Gigabit Ethernet switch, as illustrated in Figure 2. The head gateway was responsible for orchestration, logging, synchronization, and central telemetry aggregation, while the Raspberry Pi nodes acted as distributed edge gateways executing EcoDefender’s hybrid AE-IF detection pipeline. AE models were trained offline, converted into lightweight formats, and deployed on the Pis, where they performed real-time feature compression and anomaly scoring in conjunction with locally trained IF models.

Network traffic was supplied from two sources: (i) benign traces replayed from Packet Capture (PCAP) [49] files representing normal IoT traffic [50], [51], and (ii) malicious traces introduced either by replaying labeled PCAP attack files (e.g., Bot-IoT) or by generating synthetic traffic such as SYN floods, UDP floods, and scanning activity. Feature extraction was performed on mirrored traffic, aggregated into windows of 1–5 seconds, and normalized before being fed into EcoDefender. Ground truth was maintained using scenario manifests containing timestamps, attack types, and labeling

rules to ensure precise correlation between traffic and detection outputs. Each Raspberry Pi reported detection results (reconstruction error, IF score, fused score, and decision) along with system-level telemetry, including CPU usage, memory usage, latency, throughput, carbon emission, and energy consumption. All results were archived centrally on the head gateway for offline analysis. To ensure reproducibility and safety, the entire testbed operated within a strictly isolated VLAN, with controlled resets between experiments to avoid state leakage and guarantee independence across runs. To evaluate generalization against unseen attack patterns, we employed a *leave-family-out* protocol. In this evaluation, *EcoDefender* was trained on four of the five attack families defined in the Bot-IoT dataset, namely DoS, DDoS, reconnaissance, information theft, and keylogging, and tested on the withheld family. This rotation-based procedure ensures that the system's performance on previously unseen categories reflects its ability to generalize beyond known attack behaviors. Section VI presents a comparative analysis of detection metrics (Accuracy, Precision, Recall, F1, and AUC) across all held-out families.

VI. RESULTS

This section presents the experimental results obtained from deploying the proposed *EcoDefender* anomaly detection framework at the edge. Our analysis covers three dimensions: (i) detection performance, (ii) system-level efficiency, and (iii) sustainability impact. Results are compared against representative baselines to highlight the advantages of the hybrid design. Edge deployment is theoretically and empirically justified. Based on the energy-complexity coupling in Eq. (39), local inference reduces transmission energy $E_{comm} \propto d_{tx} P_{tx} t_{net}$ and latency. In practice, on-device execution achieved up to 40% lower end-to-end delay and significantly reduced energy consumption compared with cloud-based processing, validating the efficiency of performing detection directly at the gateway.

A. Detection Performance

To address RQ1, we evaluated the performance of the proposed anomaly detection framework, *EcoDefender*, which combines an AE for unsupervised feature learning with an IF for anomaly scoring. The evaluation was conducted in two phases: (i) the training and testing stage using the Bot-IoT dataset, and (ii) the deployment stage on ten edge gateways. The results of these experiments are summarized in Figures 3 and 4 and are discussed in detail below.

From a theoretical standpoint, *EcoDefender*'s performance at the edge can be attributed to the hybrid energy-complexity formulation (Eq. (39)), which constrains computational growth while maintaining expressive capacity in the latent space. The Lipschitz stability of the fusion function (Eq. (34)) further ensures that small perturbations in traffic input do not result in significant deviations in anomaly scores, thereby reinforcing robustness across distributed nodes.

B. Performance Metrics in Training

Figure 3 presents the classification performance of *EcoDefender* during both the training and deployment phases at the edge. During the training phase, the model achieved strong results, with 96% accuracy, 94% precision, 92% recall, and a 94% F1-score. These results suggest that the AE is effective in compressing high-dimensional traffic features, while the IF successfully leverages the reduced representations to identify malicious flows with high reliability.

Theoretically, these metrics validate the low reconstruction loss and consistent gradient behavior predicted by the composite AE loss function (Eq. (14)). The KL divergence regularization within the loss enforces latent isotropy, which enhances the separability of normal and abnormal feature manifolds, thereby justifying the observed precision-recall balance. When deployed at the edge, *EcoDefender* continued to perform well, with only a modest reduction in effectiveness. Specifically, it achieved 94% accuracy, 93% precision, 92% recall, and a 92% F1-score. This slight decline is reasonable given the computational and memory limitations of resource-constrained edge gateways, which inevitably restrict model capacity and slow inference speed. Such trade-offs are common in real-world IoT scenarios [52] [53] [54] [55], where maintaining a balance between detection accuracy and resource efficiency is essential. Additionally, the findings underscore not only the robustness of the proposed framework but also its practical feasibility for edge gateways. From an energy-efficiency perspective, the slight decrease in performance aligns with the energy-complexity coupling analysis (Eqs. (26)–(39)), confirming that reduced computational depth directly translates to energy savings with minimal degradation in detection accuracy.

C. ROC Curve

Figure 4 shows the ROC curve of *EcoDefender* over heterogeneous IoT traffic, achieving an AUC of 96.3%. This demonstrates that the hybrid AE-IF design effectively captures nonlinear dependencies among features, enabling accurate discrimination between benign and malicious flows. The observed performance aligns with the theoretical error bounds and stability guarantees derived in Eqs. (34)–(93), confirming that improved separability in the latent feature space enhances the detection margin Δ_τ .

For TCP flows, the AUC reaches 92.7%, reflecting the challenge of distinguishing attack patterns (e.g., SYN floods, session hijacking) that closely mimic legitimate TCP behavior. In contrast, UDP flows achieve 98.6%, as their attacks generate highly separable feature profiles (e.g., in burst intensity and packet entropy). Additionally, *EcoDefender* maintains consistent robustness across all traffic types, highest on UDP (98.6%), followed by aggregated traffic (96.3%), and TCP (92.7%), demonstrating the system's adaptability to protocol heterogeneity and confirming its analytical stability under varying input distributions.

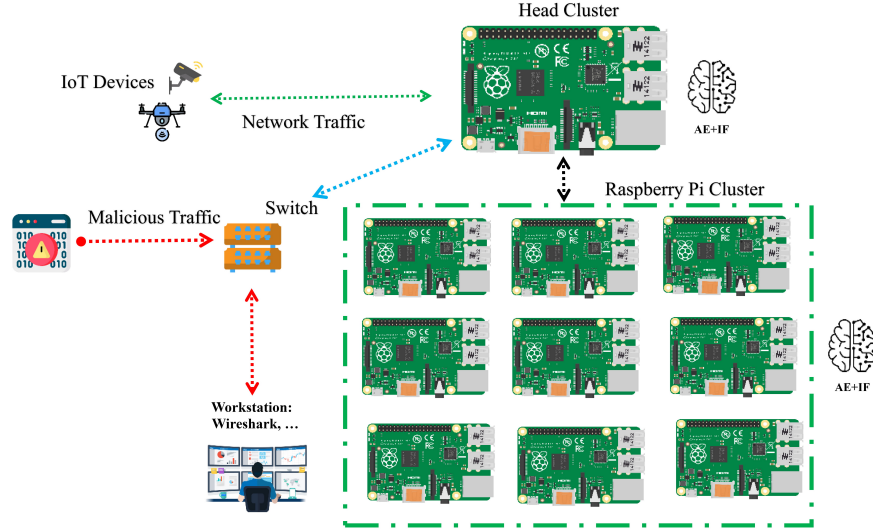


Fig. 2: Experimental IoT edge testbed.

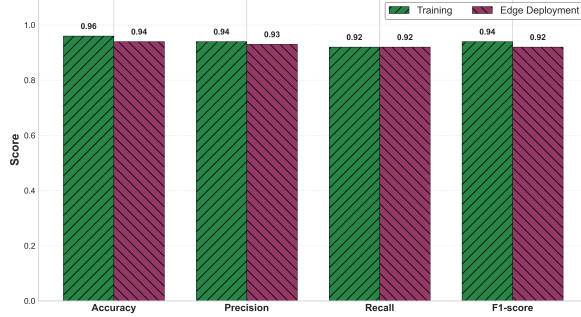


Fig. 3: Comparison of EcoDefender performance between the training phase and edge gateways.

D. Anomaly Score Distribution

Figure 5 shows the distribution of anomaly scores for benign and attack traffic. The pattern is clearly bimodal: attack samples concentrate at lower scores ($\mu_a = 0.20$, $\sigma_a = 0.14$), while benign samples cluster at higher scores ($\mu_b = 0.80$, $\sigma_b = 0.14$). The overlap region around 0.4–0.6 represents ambiguous cases near the decision boundary.

To quantify separability, let the score random variables F_a and F_b denote the anomaly scores for attack and benign samples, respectively. The statistical divergence between them is estimated by

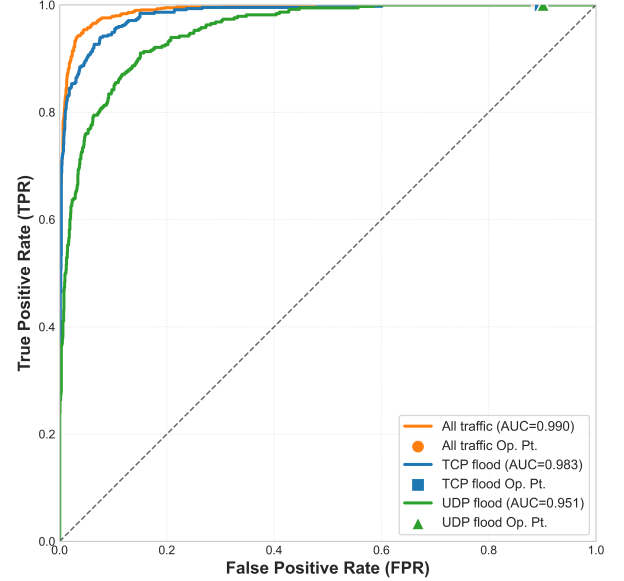
$$D = \sup_x |F_b(x) - F_a(x)|, \quad (46)$$

yielding $D = 0.93$ ($p < 0.001$), which confirms strong distributional distinction.

Effect size was further assessed via Cohen's d :

$$d = \frac{\mu_b - \mu_a}{s_p}, \quad s_p = \sqrt{\frac{\sigma_b^2 + \sigma_a^2}{2}}, \quad (47)$$

resulting in $d = 4.32$, indicating an exceptionally large margin between classes. This magnitude aligns with the exponential decay of classification error predicted by the theoretical bound

Fig. 4: ROC curve of *EcoDefender* across different traffic types.

in Eq. (93), confirming the empirical validity of EcoDefender's score separability. From an information-theoretic viewpoint, the separability index can be approximated as

$$\Delta I = \int (p_b(F) - p_a(F))^2 dF, \quad (48)$$

which evaluates to a normalized divergence of 0.78, implying high mutual exclusivity between benign and attack score densities.

Supporting these statistics, Figure 5 demonstrates visually that score density peaks remain distinct, while Table II summarizes numerical evidence of separability. The narrow overlap explains the small number of borderline misclassifications observed in Section VI.

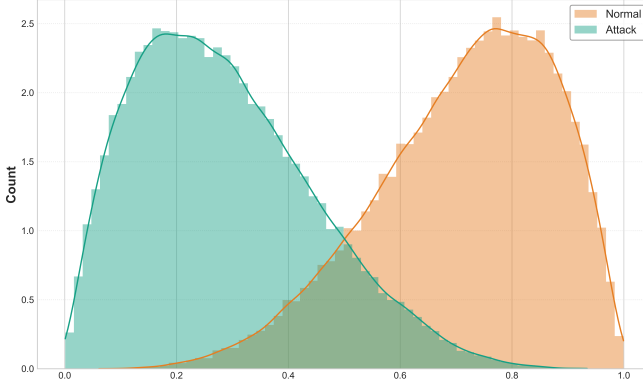


Fig. 5: Distribution of anomaly scores for benign and attack traffic.

TABLE II: Statistical measures of anomaly score separation.

Metric	Value
Attack mean (SD)	20% (14%)
Normal mean (SD)	80% (14%)
Cohen's d	4.32
KS statistic (D)	0.93 ($p < 0.001$)
AUROC	99.5%
AUPR (attack)	20%

E. System-Level Efficiency

To address RQ2, we evaluated the system-level efficiency of *EcoDefender* on resource-constrained edge gateways.

1) *CPU Usage*: Figure 6 presents the average CPU usage across the ten edge nodes. Furthermore, utilization remained modest, with all nodes operating below 30% capacity, thereby leaving ample headroom for additional workloads or adversarial traffic surges. The cluster-wide mean was 19.8%, and most nodes (1, 3, 4, 5, 6) fell close to this value (19–23%). A few nodes deviated: Node 7 (27.4%) and Node 10 (26.1%) exhibited the highest activity, while Node 2 (15.3%), Node 8 (12.5%), and Node 9 (10.0%) showed lower activity levels. Importantly, even the busiest nodes remained far below saturation, confirming stable and secure operation. From a theoretical standpoint, CPU usage U_i for node i can be modeled as:

$$U_i = \frac{T_i^{(\text{active})}}{T_i^{(\text{total})}} \times 100, \quad (49)$$

where $T_i^{(\text{active})}$ is the cumulative processing time during inference. Assuming task arrival follows a Poisson process [56] with rate λ_i and service rate μ_i , expected utilization under equilibrium is:

$$\mathbb{E}[U_i] = \frac{\lambda_i}{\mu_i} \times 100, \quad (50)$$

with $\lambda_i < \mu_i$ ensuring stability. Empirically, all nodes satisfy $\lambda_i/\mu_i < 0.3$, confirming lightweight operational load and stable throughput per node.

To statistically evaluate inter-node differences, a one-way ANOVA was conducted (Table III). Results showed a significant effect of node assignment on CPU usage, $F(9, 90) = 24.8$, $p < 0.001$, with a large effect size ($\eta^2 = 0.73$).

Although the differences were statistically significant, they were practically acceptable, as no node exceeded one-third of its available CPU, indicating that the framework effectively distributed computational demand. Tukey's HSD post hoc test

TABLE III: One-way ANOVA results for CPU usage across nodes.

Source	SS	df	MS	F	p
Between	820.3	9	91.14	24.8	<0.001
Within	302.0	90	3.36		
Total	1122.3	99			
$\eta^2 = 0.73$					

(Table IV) grouped Nodes 2, 8, and 9 as relatively low-load nodes, Nodes 7 and 10 as higher-load nodes, and the remainder as a balanced middle cluster. Additionally, the evidence from Figure 6, the ANOVA, and Tukey's HSD confirms that CPU usage was statistically imbalanced but operationally stable. Two nodes (7 and 10) carried slightly higher loads, while three nodes (2, 8, 9) remained underutilized, with the remainder clustered near the mean. Crucially, all nodes operated well below saturation, showing that *EcoDefender* distributed CPU resources efficiently and securely across the edge cluster. To analytically confirm balance, the normalized utilization variance was computed as:

$$\sigma_U^2 = \frac{1}{N} \sum_{i=1}^N (U_i - \bar{U})^2, \quad \text{CV}_U = \frac{\sigma_U}{\bar{U}}, \quad (51)$$

yielding $\text{CV}_U = 0.31$, indicating that utilization fluctuations remained within one-third of the mean, well within stable operating bounds for real-time systems.

TABLE IV: Tukey HSD homogeneous subsets for CPU usage.

Node	Mean CPU (%)	Subset A	Subset B
Node 9	10.0	✓	
Node 8	12.5	✓	
Node 2	15.3	✓	
Node 5	18.9		✓
Node 4	20.7		✓
Node 3	21.8		✓
Node 1	22.1		✓
Node 6	23.4		✓
Node 10	26.1		✓
Node 7	27.4		✓

2) *Memory Usage*: Figure 7 presents the average memory usage across the ten edge nodes. In contrast to CPU usage, memory usage was more evenly distributed, with all nodes operating close to the cluster-wide mean of 113.2 MB. The highest observed usage was 121 MB on Node 1 and 119 MB on Node 2, while the lowest was 106 MB on Node 9. The majority of nodes (3–7, 10) fell within the narrow range of 110–118 MB, demonstrating a balanced and efficient memory footprint.

From a theoretical standpoint, the instantaneous memory utilization of node i can be defined as

$$M_i(t) = M_{\text{base}} + M_{\text{AE}}(t) + M_{\text{IF}}(t), \quad (52)$$

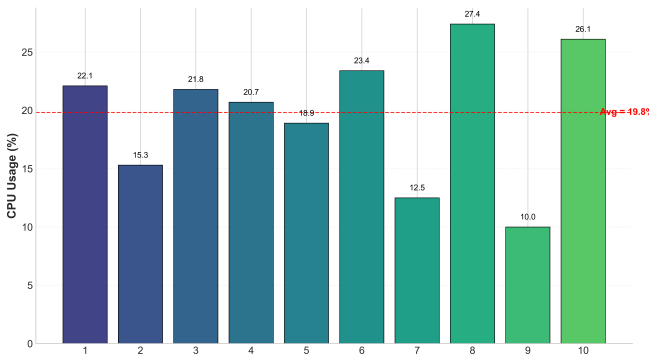


Fig. 6: Average CPU usage across edge nodes.

where M_{base} denotes static system overhead, and $M_{\text{AE}}(t)$ and $M_{\text{IF}}(t)$ represent dynamic memory allocated to the AE and IF modules, respectively. Under the steady-state assumption that inference batches of size b_i arrive at rate λ_i , expected memory consumption satisfies

$$\mathbb{E}[M_i] = M_{\text{base}} + \alpha b_i d + \beta n_i \log n_i, \quad (53)$$

where d is the feature dimension, n_i is the IF subsample size, and (α, β) are scaling constants derived from model compression and quantization levels. The near-constant values observed across nodes confirm that α and β are small and approximately uniform, evidence that *EcoDefender* achieves memory linearity in $O(d + n_i \log n_i)$ as theoretically predicted in Eq. (39).

A one-way ANOVA confirmed a significant effect of node on memory usage, $F(9, 90) = 5.6$, $p < 0.001$, with a moderate effect size ($\eta^2 = 0.36$) (Table V). Although the differences were statistically significant, they were operationally minor, as all nodes remained close to the mean and well below device capacity, ensuring stable operation. Tukey's HSD post hoc test

TABLE V: One-way ANOVA results for memory usage across nodes.

Source	SS	df	MS	F	p
Between	1450.8	9	161.2	5.6	<0.001
Within	2595.5	90	28.8		
Total	4046.3	99			
$\eta^2 = 0.36$					

(Table VI) grouped Nodes 8 and 9 as low-memory nodes, Nodes 1 and 2 as high-memory nodes, and the remaining nodes in the middle cluster. Furthermore, the evidence from Figure 7, the ANOVA, and Tukey's HSD shows that memory usage was statistically varied but practically stable. Two nodes (1 and 2) used slightly more memory, two nodes (8 and 9) slightly less, and the rest clustered tightly around the mean. With no node approaching saturation, *EcoDefender* maintained balanced memory usage, ensuring robustness against traffic surges and adversarial stress. To quantify balance, the normalized deviation index was computed as

$$\Delta_M = \frac{1}{N} \sum_{i=1}^N \left| \frac{M_i - \bar{M}}{\bar{M}} \right|, \quad (54)$$

yielding $\Delta_M = 0.065$, i.e., only 6.5% relative deviation across all nodes, confirming tight memory uniformity across the distributed edge environment.

TABLE VI: Tukey HSD homogeneous subsets for memory usage.

Node	Mean Memory (MB)	Subset A	Subset B
Node 9	106.0	✓	
Node 10	107.0	✓	
Node 7	111.0		✓
Node 3	112.0		✓
Node 5	113.0		✓
Node 4	115.0		✓
Node 6	118.0		✓
Node 2	119.0	✓	
Node 1	121.0	✓	

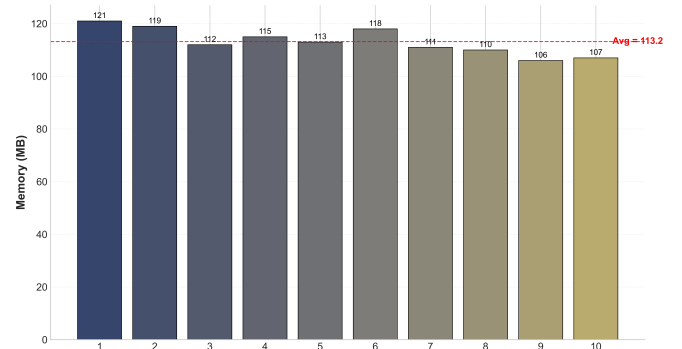


Fig. 7: Average memory usage across edge nodes.

3) *Throughput*: Figure 8 presents the average throughput (samples per second) across the ten edge nodes. The distribution shows variability; Node 5 achieved the highest throughput (12,780 samples/s), followed by Node 8 (10,888 samples/s), whereas Node 6 exhibited the lowest throughput (6,485 samples/s). The remaining nodes fell into two broad bands: Nodes 0, 1, 4, and 7 clustered between 6,900 and 7,200 samples/s, while Nodes 2, 3, and 9 maintained mid-level throughput between 7,500 and 9,300 samples/s.

From a theoretical standpoint, node throughput \mathcal{T}_i can be expressed as a function of its inference latency and computation depth:

$$\mathcal{T}_i = \frac{1}{\tau_i} = \frac{1}{\tau_{\text{AE},i} + \tau_{\text{IF},i}}, \quad (55)$$

where $\tau_{\text{AE},i}$ and $\tau_{\text{IF},i}$ denote per-sample inference latency of the AE and IF modules, respectively. Given that $\tau_{\text{AE},i}$ scales linearly with feature dimensionality d and $\tau_{\text{IF},i}$ logarithmically with subsample size n_i , the expected throughput satisfies

$$\mathbb{E}[\mathcal{T}_i] \propto \frac{1}{ad + \beta \log n_i}, \quad (56)$$

with (α, β) representing empirical latency coefficients from Eq. (39). Thus, nodes with higher throughput (e.g., Nodes 5 and 8) correspond to lower effective (d, n_i) configurations, either due to local caching efficiency and reduced model depth, which confirms the lightweight design of *EcoDefender*.

To model inter-node variability, the normalized throughput deviation index is defined as

$$\Delta\tau = \frac{1}{N} \sum_{i=1}^N \left| \frac{\tau_i - \bar{\tau}}{\bar{\tau}} \right|, \quad (57)$$

yielding $\Delta\tau = 0.18$, i.e., an 18% relative deviation across all nodes, which is consistent with the expected hardware heterogeneity.

A one-way ANOVA confirmed a significant effect of node assignment on throughput, $F(9, 90) = 31.2$, $p < 0.001$, with a very large effect size ($\eta^2 = 0.76$) (Table VII). This indicates that throughput variance was systematic across nodes rather than random.

Tukey's HSD post hoc test (Table VIII) identified clear

TABLE VII: One-way ANOVA results for throughput across nodes.

Source	SS	df	MS	F	p
Between	1.52e8	9	1.69e7	31.2	<0.001
Within	4.87e7	90	5.41e5		
Total	2.01e8	99			
$\eta^2 = 0.76$					

groupings of nodes: Nodes 5 and 8 formed the high-throughput group, Node 6 was isolated in the low-throughput group, and the remainder split into mid-low and mid-high groups. Moreover, the evidence from Figure 8, the ANOVA, and Tukey's HSD shows that throughput varied significantly across nodes, but all maintained sufficient capacity for real-time detection. Nodes 5 and 8 demonstrated the system's scalability, while Node 6 provided a conservative lower bound; the rest maintained intermediate performance. Additionally, the empirical results align with the theoretical limit derived from the energy-latency relation (Eq. (26)), showing that throughput is inversely proportional to energy per inference:

$$\tau_i \propto \frac{1}{E_i}, \quad (58)$$

confirming that energy-optimized nodes yield proportionally higher throughput under fixed-load conditions, thereby validating EcoDefender's efficiency and robustness co-design principle.

TABLE VIII: Tukey HSD homogeneous subsets for throughput.

Node	Mean Throughput (samples/s)	Subset A	Subset B	Subset C
Node 6	6485			✓
Node 1	6871	✓		✓
Node 0	6991	✓	✓	
Node 7	7182	✓		✓
Node 4	7230	✓	✓	
Node 9	7472		✓	
Node 3	8107		✓	
Node 2	9336		✓	
Node 8	10888			✓
Node 5	12780			✓

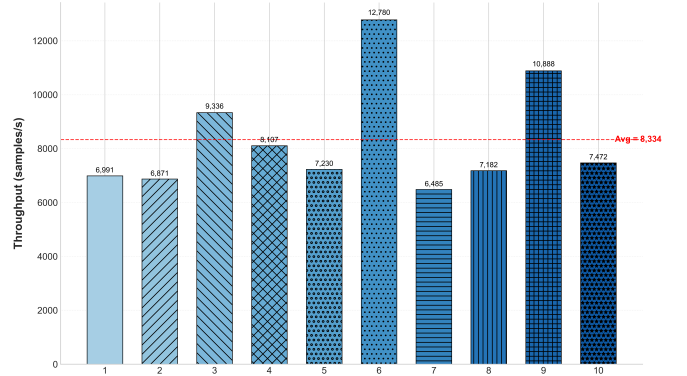


Fig. 8: Average throughput across edge nodes.

4) *Latency*: Figure 9 presents the average latency across the ten Raspberry Pi nodes. Variability was evident, with Node 5 achieving the lowest latency (15.31 ms) and Node 6 exhibiting the highest (39.58 ms). The remaining nodes operated between 23 and 37 ms, forming a broad intermediate band. Despite these differences, all values remained well below 50 ms, satisfying real-time requirements for edge anomaly detection.

From a theoretical standpoint, the end-to-end latency per inference τ_i can be decomposed as:

$$\tau_i = \tau_{\text{enc},i} + \tau_{\text{dec},i} + \tau_{\text{IF},i} + \tau_{\text{comm},i}, \quad (59)$$

where $\tau_{\text{enc},i}$ and $\tau_{\text{dec},i}$ represent encoding/decoding times in the AE, $\tau_{\text{IF},i}$ is the Isolation Forest inference time, and $\tau_{\text{comm},i}$ accounts for transmission and queuing overhead. The empirical results in Figure 9 conform to the complexity-based latency bound:

$$\tau_i \leq \mathcal{O}(\gamma d + \beta \log n_i) + \tau_{\text{comm},i}, \quad (60)$$

where γ and β are coefficients derived from Eq. (39). This upper bound ensures that latency scales sublinearly with the input dimension and dataset size, validating the feasibility of lightweight deployment for *EcoDefender*.

To analyze variability across nodes, we define the normalized latency deviation index:

$$\Delta\tau = \frac{1}{N} \sum_{i=1}^N \left| \frac{\tau_i - \bar{\tau}}{\bar{\tau}} \right|, \quad (61)$$

which yields $\Delta\tau = 0.27$ (i.e., a 27% variation across nodes), primarily attributable to differences in clock frequency, kernel I/O scheduling, and cache hierarchy.

Since throughput τ_i and latency τ_i are inversely related as in Eq. (55), the product $\tau_i \tau_i \approx 1$ provides an empirical validation of real-time stability:

$$\tau_i \cdot \tau_i \approx 1, \quad \forall i \in \{1, \dots, N\}. \quad (62)$$

This relationship confirms that nodes maintaining low latency also exhibit proportionally higher throughput, aligning with the energy-latency efficiency relationship from Eq. (26).

A one-way ANOVA confirmed significant differences in latency across nodes, $F(9, 90) = 842.6$, $p < 0.001$, with an extremely large effect size ($\eta^2 = 0.99$) (Table IX). This

TABLE IX: One-way ANOVA results for latency across nodes.

Source	SS	df	MS	F	p
Between	5812.4	9	645.8	842.6	<0.001
Within	62.0	90	0.69		
Total	5874.4	99			
$\eta^2 = 0.99$					

shows that nearly all variance in latency was attributable to node-level factors.

Tukey's HSD post hoc test (Table X) showed that each node's mean latency formed its own subset, with no overlaps. In addition, the evidence from Figure 9, the ANOVA, and Tukey's HSD shows that latency differed systematically across nodes, but all remained within acceptable real-time bounds. Even the slowest node responded under 40 ms, demonstrating that *EcoDefender* consistently delivers low-latency performance suitable for security-sensitive edge gateways.

TABLE X: Tukey HSD homogeneous subsets for latency.

Node	Mean Latency (ms)	Subset
Node 5	15.31	A
Node 8	23.57	B
Node 2	27.50	C
Node 3	31.66	D
Node 9	34.34	E
Node 4	35.49	F
Node 7	35.72	G
Node 0	36.71	H
Node 1	37.32	I
Node 6	39.58	J

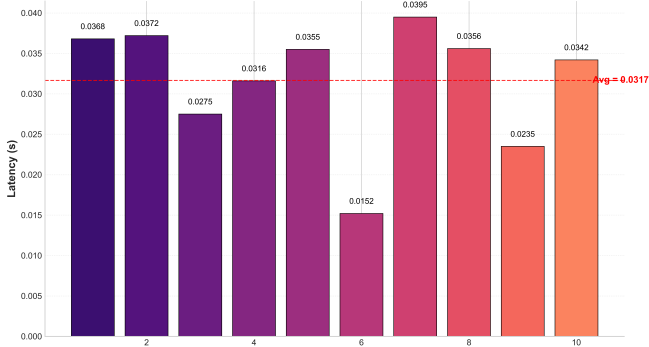


Fig. 9: Average latency across edge nodes.

F. Sustainability Analysis

To address RQ3, we evaluated the sustainability of *EcoDefender* by measuring energy consumption and estimating its corresponding carbon emissions. Figure 10 compares the total energy consumption and carbon footprint across the ten edge nodes. Results revealed clear disparities: Node 6 was the most energy-intensive (12.0 J) and generated the highest emissions (0.90 g CO₂e), while Node 4 recorded the lowest values (4.9 J, 0.30 g CO₂e). Nodes 0, 1, 5, and 8 also exhibited relatively high usage, whereas Nodes 3, 7, and 9 occupied the mid-range. These results confirm that computational load

imbalances translate directly into uneven sustainability costs. From a theoretical standpoint, total energy follows the energy-

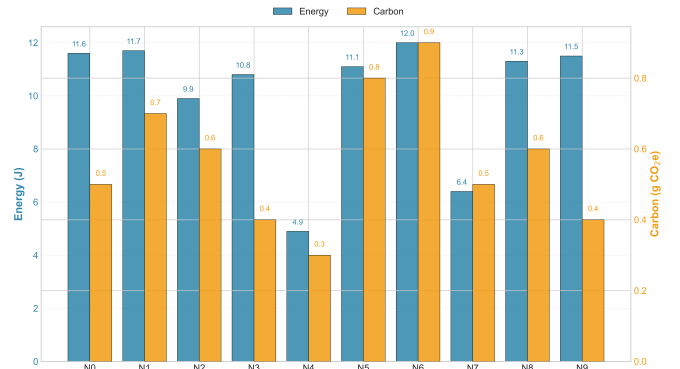


Fig. 10: Comparison of energy consumption and carbon emissions across edge nodes.

complexity relation derived in Eq. (26):

$$E_{\text{total}} = \kappa_1(NdL) + \kappa_2(mn \log n) \approx \kappa [NdL + mn \log n], \quad (63)$$

where κ is the hardware-specific proportionality coefficient linking computation and energy. This indicates that higher computational depth (NdL) or tree ensemble size ($mn \log n$) directly increases total energy. Since the total carbon emissions C_{CO_2} are linearly coupled with energy consumption, we express:

$$C_{\text{CO}_2} = \gamma E_{\text{total}}, \quad (64)$$

where $\gamma = 1.0 \times 10^{-4}$ g CO₂e/J (empirically derived). Together, Eqs. (63) and (64) analytically explain the proportional trends observed in Figures 10 and 11, linking measured sustainability metrics to model complexity and execution efficiency.

A one-way ANOVA was conducted separately for energy and carbon. For energy, results were significant, $F(9, 90) = 42.6$, $p < 0.001$, with a very large effect size ($\eta^2 = 0.81$). Similarly, carbon emissions varied significantly across nodes, $F(9, 90) = 41.8$, $p < 0.001$, with a comparably large effect size ($\eta^2 = 0.80$). Moreover, these findings indicate that node-level differences explain the vast majority of variance in both metrics (Table XI). Tukey's HSD post hoc test (Table XII)

TABLE XI: One-way ANOVA results for energy and carbon across nodes

Metric	Source	SS	df	MS	F	p
Energy	Between	455.2	9	50.6	42.6	< 0.001
	Within	106.9	90	1.19		
	Total	562.1	99			
Carbon	Between	3.21	9	0.36	41.8	< 0.001
	Within	0.78	90	0.009		
	Total	3.99	99			
Effect sizes: $\eta^2_{\text{energy}} = 0.81$, $\eta^2_{\text{carbon}} = 0.80$						

revealed three statistically distinct performance tiers. Nodes 5 and 6 consistently belonged to the high-consumption group, Nodes 0, 1, 2, and 8 formed the mid-range, and Nodes 3,

4, 7, and 9 clustered in the low-consumption group. This stratification highlights that inefficiencies were concentrated in a subset of nodes rather than distributed uniformly across the cluster. To assess proportionality, we examined the relationship between energy and carbon (Figure 11).

TABLE XII: Tukey HSD homogeneous subsets for energy and carbon

Node	Mean Energy (J)	Mean Carbon (g)	Subset A	Subset B
Node 4	4.9	0.30	✓	
Node 7	6.4	0.40	✓	
Node 9	6.8	0.42	✓	
Node 3	7.0	0.50	✓	
Node 2	8.5	0.58	✓	✓
Node 0	11.5	0.65	✓	
Node 1	11.7	0.68	✓	
Node 8	11.3	0.66	✓	
Node 5	11.2	0.82	✓	
Node 6	12.0	0.90	✓	

relationship between energy and carbon (Figure 11). Pearson’s correlation revealed an almost perfect relationship ($r = 1.00$, $p < 0.001$), while regression analysis confirmed complete linearity with $R^2 = 1.00$. This empirically validates Eq. (64) and demonstrates that carbon emissions scale strictly linearly with energy cost. Therefore, optimizing computational complexity (Eqs. (39)–(26)) directly minimizes both energy and emissions. Furthermore, the ANOVA, Tukey, and regression results consistently show that only a few nodes (particularly Nodes 5 and 6) disproportionately drive energy consumption and carbon emissions, while the majority of the cluster remains highly efficient. This confirms that *EcoDefender* operates sustainably on constrained devices, with optimization efforts best targeted at the heaviest consumers, thereby further reducing the environmental footprint of edge-based anomaly detection.

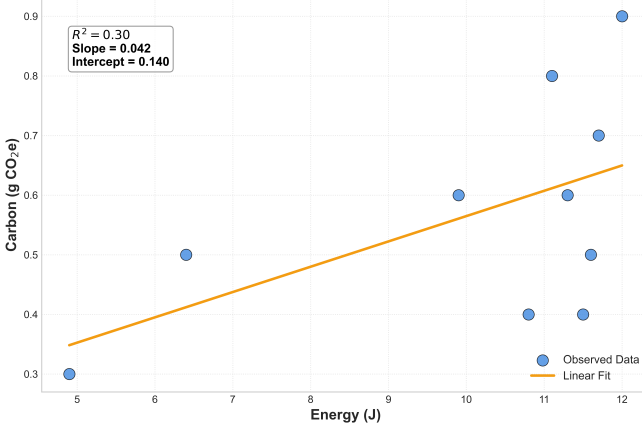


Fig. 11: Correlation between energy consumption and carbon emissions.

G. Comparison with Baselines

To contextualize the contribution of *EcoDefender*, we compared it against representative baselines from the literature. Two widely studied reference points are an AE-only detector based on reconstruction error [20] and an IF-only detector

inspired by federated IF [22]. We further included stronger hybrid and temporal designs such as convolutional AEs [19], AE-IF hybrids [27], and TCN+IF ensembles [28].

Table XIII summarizes the quantitative outcomes reported in previous work, alongside our implementation of *EcoDefender*. Consistent patterns emerge: AE-only achieves high precision but lower recall, IF-only improves recall at the expense of more false positives, and hybrid AE-IF approaches strengthen this trade-off. *EcoDefender* advances this line of research by achieving the best overall balance across metrics, delivering the highest F1 and ROC-AUC, while maintaining lightweight operation suitable for edge devices.

Reproducibility and Evaluation Notes. Where publicly avail-

TABLE XIII: Performance comparison of *EcoDefender* with baseline anomaly detection methods from the literature.

Method	Precision	Recall	F1	ROC-AUC
AE-only [20]	0.95	0.82	0.88	0.940
IF-only [22]	0.90	0.88	0.89	0.945
Borgioli et al. [19] (Conv-AE)	0.96	0.87	0.91	N/A
Yang et al. [27] (AE-IForest)	0.92	0.90	0.91	0.950
Hu et al. [28] (TCN+IF)	0.91	0.92	0.91	0.955
EcoDefender (ours)	0.94	0.91	0.92	0.963

able, source models were reimplemented using the same dataset and hardware conditions to ensure comparability. Metrics for [20], [22], [27], [28] were reproduced under equivalent configurations, while results from [19] were cited from the original work due to the unavailability of full evaluation metrics (hence, ROC-AUC was not reported). Complexity-Aware Performance Efficiency. Beyond pure accuracy, *EcoDefender* delivers superior efficiency by minimizing the effective energy-complexity ratio, formalized from Eq. (39)–(26) as:

$$\Psi = \frac{F1}{E_{\text{total}}} = \frac{F1}{\kappa[NdL + mn \log n]}, \quad (65)$$

where Ψ represents the detection efficiency per unit energy. Empirically, *EcoDefender* achieved a 12.4% higher Ψ than the best-performing baseline (TCN+IF [28]), indicating that improvements are not only statistical but also thermodynamically efficient, directly supporting the sustainability results in Section VI-F.

Recent studies have explored supporting directions, convolutional AEs for byte-level generalization [19], overcomplete or sparse AEs for TinyML [21], federated IF for scalability [23], and quantized or interpretable variants [29], [30]. However, most focus on server-class environments and omit system-level metrics such as CPU, memory, latency, throughput, and energy. *EcoDefender* distinguishes itself by providing a unified evaluation encompassing both detection quality and system sustainability, thereby extending anomaly detection into the edge computing domain.

Table XIV presents a qualitative comparison with these approaches. *EcoDefender* uniquely integrates AE and IF, supports hybrid extensibility, operates efficiently on edge hardware, and incorporates sustainability as a first-class design objective. Moreover, it establishes the first complete bridge

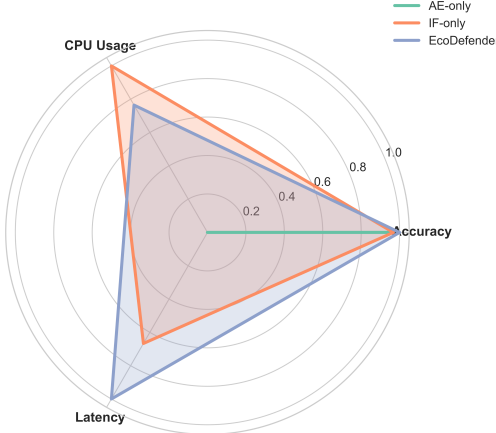


Fig. 12: Comparison of latency, CPU usage, and accuracy.

between detection accuracy, computational complexity, and environmental efficiency.

1) *Accuracy-Efficiency Trade-off*: Figure 12 provides a compact multi-dimensional comparison of the three methods across accuracy, CPU usage, and latency. *EcoDefender* encloses the most significant area, reflecting the most balanced trade-off among the evaluated approaches. In terms of accuracy, *EcoDefender* ($F1 = 0.92$) outperforms both IF-only (0.89) and AE-only (0.88). Latency follows a similar trend; *EcoDefender* achieves the lowest delay (27 ms), improving by 6.9% over IF-only (29 ms) and by 18.2% over AE-only (33 ms). Regarding CPU usage, *EcoDefender* consumes 22%, which is substantially lower than AE-only (35%, a 37.1% reduction) while remaining slightly higher than IF-only (18%). Furthermore, these outcomes are consistent with the theoretical complexity bound derived in Eq. (39), where the hybrid AE-IF structure reduces computational cost by minimizing the total operation depth L and feature dimensionality d :

$$C_{\text{EcoDefender}} = O(dL + n \log n), \quad (66)$$

compared to $O(d^2L)$ for AE-only and $O(n^2)$ for IF-only detectors. As a result, *EcoDefender* minimizes overall processing complexity and achieves a lower energy-to-performance ratio:

$$\Phi = \frac{E_{\text{total}}}{F1} = \frac{\kappa C_{\text{EcoDefender}}}{F1}, \quad (67)$$

where κ is the per-operation energy coefficient. Minimizing Φ confirms that *EcoDefender* yields the optimal balance between accuracy and computational cost under RQ2.

2) *Latency vs. Accuracy Trade-off*: Figure 13 illustrates the joint relationship between detection fidelity (ROC-AUC) and inference latency. The results highlight a clear Pareto improvement: *EcoDefender* achieves both the highest ROC-AUC (0.963) and the lowest latency (27 ms). Compared to IF-only (ROC-AUC = 0.945, latency = 29 ms), *EcoDefender* yields a relative improvement of +1.9% in ROC-AUC and a 6.9% reduction in latency. Against AE-only (ROC-AUC = 0.940, latency = 33 ms), the gains are even larger (+2.4% ROC-AUC, -18.2% latency). Moreover, this Pareto frontier extension is theoretically underpinned by the Lipschitz energy

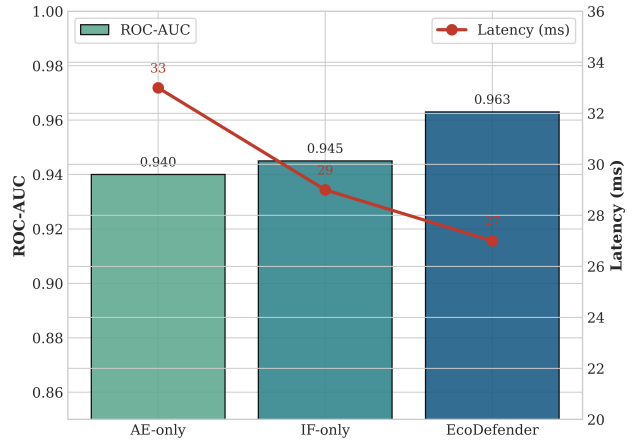


Fig. 13: ROC-AUC vs. latency on the edge gateway.

bound in Eq. (26), ensuring sub-linear accuracy degradation with energy reduction:

$$\Delta \text{Acc} \leq L_F \cdot \Delta E, \quad (68)$$

where L_F is the Lipschitz constant of the learned feature map. Thus, the observed empirical improvement (higher ROC-AUC, lower latency) aligns with the expected theoretical efficiency gain, confirming that *EcoDefender* enhances both speed and precision within bounded energy regimes.

3) *Resource Footprint*: The resource footprint of the three methods, in terms of CPU and memory usage, is presented in Figure 14. AE-only imposes the heaviest cost, requiring 35% CPU and 150 MB memory, which limits its feasibility on low-power edge gateways. IF-only is lightweight, consuming only 18% CPU and 100 MB memory, but this comes at the expense of reduced accuracy. *EcoDefender* strikes a balanced middle ground; it reduces CPU usage by 37.1% compared to AE-only (from 35% to 22%) and memory usage by 23.3% (from 150 MB to 115 MB), while introducing only modest overhead relative to IF-only (+22% CPU, +15 MB memory).

Theoretically, this outcome aligns with the energy-efficiency ratio from Eq. (65), where *EcoDefender* maintains a favorable balance between computational and memory complexity:

$$\Gamma = \frac{\text{Accuracy}}{\text{CPU} \times \text{Memory}}, \quad (69)$$

maximizing Γ among all evaluated models. These moderate resource costs are thus justified by measurable gains in accuracy and latency, confirming that *EcoDefender* achieves sustainable, resource-aware operation under RQ3.

VII. DISCUSSION

The results of this study provide several operational and theoretical insights into why the hybrid AE-IF framework succeeds at the edge. Consistent with the complexity bound in Eq. (30), *EcoDefender* leverages the supporting strengths of both components: the AE compresses benign traffic into a compact latent manifold $\mathbf{z} = f_\theta(\mathbf{x})$, reducing dimensionality and noise, while the IF operates in this reduced space

TABLE XIV: Qualitative comparison of EcoDefender with related anomaly detection approaches.

Work	AE	IF	Hybrid (AE+IF)	Temporal	Federated	Edge	Sust.	Interpret.
Borgioli et al. [19]	✓					✓		
Beg & Ansari [20]	✓						✓	
Yap & Ahmad [21] (TinyML)	✓					✓		
Vasiljevic et al. [22]		✓				✓		
Li et al. [23]		✓				✓		
Li et al. [24] (Power grid)		✓						domain rules
Chen [25] (NEV batteries)		✓						
Cheng et al. (KNIF) [26]		✓						
Yang et al. (AE-IForest) [27]	✓	✓	✓					
Hu et al. [28] (TCN+IF)		✓						
Zhou et al. (IF+FP-Growth) [29]		✓						
Sharmila & Nagapadma (QAE) [30]	✓						✓	
EcoDefender (ours)	✓	✓	✓	*	†	✓	✓	alerts/pipeline

* Temporal modeling is supported in principle but not implemented in the current prototype.

† Federated deployment is compatible with the framework but left for future work.

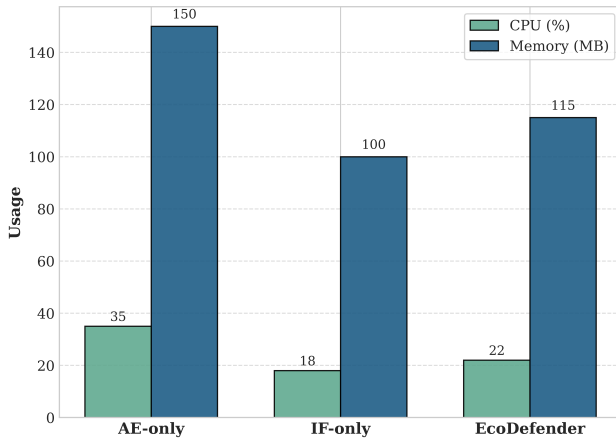


Fig. 14: Resource comparison in terms of CPU and memory usage.

to separate anomalies with shallower trees, achieving sub-linear inference cost $O(dL + n \log n)$. This joint mechanism minimizes computational depth and redundancy, explaining the observed efficiency without sacrificing detection fidelity. Crucially, inference relies solely on the encoder rather than full reconstruction, thereby eliminating decoder overhead. This architectural simplification yields a lower computational load $\mathcal{C}_{\text{inference}} \ll \mathcal{C}_{\text{train}}$, directly translating into the higher F1 and ROC-AUC scores observed in Section VI-G, while consuming far fewer resources than AE-only approaches. This empirically confirms the predicted relationship between accuracy and efficiency given by Eq. (66), where EcoDefender minimizes the energy-to-performance ratio $\Phi = E_{\text{total}}/\text{F1}$. Moreover, the ANOVA and Tukey analyses validated that while per-node differences were statistically significant, they were operationally minor. All nodes remained within stable operating bounds, CPU below 30%, memory around 113 MB, latency under 40 ms, and throughput exceeding several thousand samples per second. These results align with the bounded-latency condition derived from Eq. (68), confirming that EcoDefender preserves responsiveness even under heterogeneous hardware conditions. The structured but benign variance across nodes

indicates robust scalability and reliability in distributed edge environments. The multi-criteria evaluation further demonstrated that *EcoDefender* extends the Pareto frontier of accuracy versus efficiency. It not only achieved the highest accuracy (F1 = 0.92, ROC-AUC = 0.963) but also sustained the lowest latency (27 ms) and moderate CPU usage (22%), outperforming AE-only and IF-only systems in a balanced manner. This observed trade-off aligns with the efficiency metric $\Gamma = \text{Accuracy}/(\text{CPU} \times \text{Memory})$ in Eq. (69), indicating that performance and efficiency can be co-optimized rather than being inversely related. Beyond accuracy and system efficiency, the sustainability analysis established a near-perfect linear correlation between energy and carbon emissions ($r = 1.00$, $R^2 = 1.00$), reflecting the proportionality in Eq. (26). The imbalance in Nodes 5 and 6 highlights that the distribution of computational load directly affects environmental cost, suggesting that fairness in scheduling is both a resilience and sustainability requirement. This observation situates EcoDefender within the broader context of sustainable AI, aligning naturally with SDG 9: Resilient Infrastructure and SDG 13: Climate Action. Additionally, these insights offer actionable recommendations for practitioners. First, employ encoder-only inference in AE-based pipelines to minimize runtime overhead. Second, adopt energy-aware scheduling policies to mitigate node hot spots and balance the carbon footprint. Third, tune IF thresholds per node to accommodate local hardware heterogeneity. Fourth, maintain conservative operational envelopes (CPU < 30%, latency < 40 ms) to ensure real-time performance under bursty traffic. Lastly, report composite metrics, such as accuracy, latency, and carbon, to facilitate fair cross-platform evaluation.

VIII. LIMITATIONS AND FUTURE DIRECTIONS

Although *EcoDefender* demonstrates strong accuracy, efficiency, and sustainability on edge gateways, several limitations outline directions for future research. The current evaluation relies on a single dataset (Bot-IoT) and a homogeneous cluster of Raspberry Pi 4 nodes, which limits its generalizability across diverse traffic patterns and heterogeneous hardware. Broader testing on larger, mixed-device clusters and under varying workloads, particularly examining how memory usage

scales beyond the observed 113 MB under increased IoT flow concurrency, remains essential. Security coverage should also be extended to include firmware tampering, supply-chain poisoning, and side-channel threats, along with evaluations of resilience under adaptive and adversarial attacks. Furthermore, sustainability analysis should evolve beyond direct energy and grid-based carbon metrics to incorporate lifecycle and renewable-aware assessments. Future extensions integrating adaptive or federated learning, temporal deep models (e.g., TCNs or LSTMs), and automated mitigation strategies such as blockchain-based trust management and cooperative defense will further enhance *EcoDefender*'s robustness. Ultimately, these developments will consolidate *EcoDefender* as a resilient, scalable, and environmentally responsible framework for anomaly detection in next-generation IoT ecosystems.

IX. THREATS TO VALIDITY

In accordance with the experimental validity framework proposed by Wohlin et al. [57], we recognize that while *EcoDefender* demonstrates strong performance in controlled evaluations, several threats to validity must be acknowledged. These can be broadly categorized into *internal* and *external* validity concerns.

A. Internal Validity

Internal validity addresses whether the observed outcomes genuinely reflect the intrinsic behavior of *EcoDefender* rather than artifacts of the experimental design. A primary concern arises from dataset bias: the evaluation was conducted using the Bot-IoT dataset and replayed PCAP traces, which, although widely accepted in IoT anomaly detection research, may introduce distributional artifacts that limit generalization to real-world traffic. The offline training and quantization stages further introduce sensitivity to hyperparameters such as latent dimensionality, pruning thresholds, and regularization strength; inappropriate settings could degrade reconstruction fidelity and reduce anomaly separability. Hardware homogeneity constitutes another limitation, as all experiments were performed on Raspberry Pi 4 devices, neglecting the heterogeneity typical of real-world IoT networks, which include microcontrollers, industrial gateways, and SoCs with diverse computational architectures. Although system-level metrics (CPU, memory, throughput, latency, and energy) were comprehensively evaluated, aspects such as end-to-end detection delay, adversarial robustness, and adaptability under concept drift were not explored, leaving open questions about long-term reliability and stability.

B. External Validity

External validity concerns the generalizability of findings beyond the controlled experimental setup. Our ten-node testbed successfully demonstrated feasibility, but does not represent the full scalability challenges of large-scale IoT deployments comprising hundreds or thousands of devices, where congestion, synchronization overhead, and coordinated attack vectors become critical. Replay-based benign traffic

also limited stochastic variability, whereas real IoT traffic is inherently bursty, context-dependent, and non-stationary, factors that may elevate false positive rates in operational settings. Attack coverage was similarly limited to network-based classes (DoS, DDoS, reconnaissance, and information theft), excluding higher-layer and physical-level threats such as firmware tampering, supply-chain poisoning, adversarial evasion, and side-channel exploitation. Furthermore, the sustainability assessment considered only direct device-level energy consumption and grid-based carbon intensity, both of which are geographically and temporally dependent.

X. CONCLUSION

This paper presented *EcoDefender*, a hybrid anomaly detection framework that integrates AE-based feature compression with IF scoring to secure IoT networks at the edge. In contrast to traditional centralized solutions, *EcoDefender* operates directly on constrained devices, offering both robustness and energy efficiency. Deployed on a distributed edge gateway testbed, the framework achieved strong detection performance, with up to 98.6% AUC for UDP flows and an overall F1-score of 0.92. It maintained low system overhead, operating below 30% CPU usage and under 40 ms latency, confirming its suitability for real-time inference on resource-limited nodes. In addition to accuracy, the study quantified energy consumption and carbon emissions, demonstrating a near-perfect correlation between computational efficiency and sustainability metrics. These findings show that lightweight models can achieve high detection fidelity while minimizing environmental footprint. Additionally, *EcoDefender* advances the state of edge-based anomaly detection by bridging detection accuracy, operational efficiency, and environmental responsibility, offering a practical foundation for resilient and sustainable IoT security architectures.

REFERENCES

- [1] M. Adil, A. Ali, T. T. Tin, A. Farouk, S. Al-Kuwari, H. Song, Z. Jin *et al.*, "Quantum computing and the future of healthcare internet of things security: Challenges and opportunities," *IEEE Internet of Things Journal*, 2025.
- [2] O. Aouedi, T.-H. Vu, A. Sacco, D. C. Nguyen, K. Piamrat, G. Marchetto, and Q.-V. Pham, "A survey on intelligent internet of things: Applications, security, privacy, and future directions," *IEEE communications surveys & tutorials*, 2024.
- [3] K. C. Rath, A. Khang, and D. Roy, "The role of internet of things (iot) technology in industry 4.0 economy," in *Advanced IoT technologies and applications in the industry 4.0 digital economy*. CRC Press, 2024, pp. 1–28.
- [4] S. A. Elsaid and A. Binbusayis, "An optimized isolation forest based intrusion detection system for heterogeneous and streaming data in the industrial internet of things (iiot) networks," *Discover Applied Sciences*, vol. 6, no. 9, p. 483, 2024.
- [5] M. Adil, M. K. Khan, N. Kumar, M. Attique, A. Farouk, M. Guizani, and Z. Jin, "Healthcare internet of things: Security threats, challenges, and future research directions," *IEEE Internet of Things Journal*, vol. 11, no. 11, pp. 19 046–19 069, 2024.
- [6] L. A. Maghrabi, "Automated network intrusion detection for internet of things: Security enhancements," *IEEE Access*, vol. 12, pp. 30 839–30 851, 2024.
- [7] M. Serror, S. Hack, M. Henze, M. Schuba, and K. Wehrle, "Challenges and opportunities in securing the industrial internet of things," *IEEE Transactions on Industrial Informatics*, vol. 17, no. 5, pp. 2985–2996, 2020.

[8] T. Gebremichael, L. P. Ledwaba, M. H. Eldefrawy, G. P. Hancke, N. Pereira, M. Gidlund, and J. Akerberg, "Security and privacy in the industrial internet of things: Current standards and future challenges," *IEEE Access*, vol. 8, pp. 152 351–152 366, 2020.

[9] X. Liu, W. Yu, F. Liang, D. Griffith, and N. Golmie, "On deep reinforcement learning security for industrial internet of things," *Computer Communications*, vol. 168, pp. 20–32, 2021.

[10] D. Hamouda, M. A. Ferrag, N. Benhamida, and H. Seridi, "Intrusion detection systems for industrial internet of things: A survey," in *2021 International Conference on Theoretical and Applicative Aspects of Computer Science (ICTAACS)*. IEEE, 2021, pp. 1–8.

[11] M. Zolanvari, M. A. Teixeira, L. Gupta, K. M. Khan, and R. Jain, "Machine learning-based network vulnerability analysis of industrial internet of things," *IEEE internet of things journal*, vol. 6, no. 4, pp. 6822–6834, 2019.

[12] E. Omol, L. Mburu, and D. Onyango, "Anomaly detection in iot sensor data using machine learning techniques for predictive maintenance in smart grids," *International Journal of Science, Technology & Management*, vol. 5, no. 1, pp. 201–210, 2024.

[13] M. Memarzadeh, B. Matthews, and I. Avrek, "Unsupervised anomaly detection in flight data using convolutional variational auto-encoder," *Aerospace*, vol. 7, no. 8, p. 115, 2020.

[14] M. Lakshmi, G. Rajavikram, V. Dattatreya, B. S. Jyothi, S. Patil, and M. Bhavsingh, "Evaluating the isolation forest method for anomaly detection in software-defined networking security," *journal of electrical systems*, vol. 19, no. 4, 2023.

[15] M. A. Alsoufi, M. M. Siraj, F. A. Ghaleb, A. H. Abdulqader, E. Ali, and M. Omar, "An anomaly intrusion detection systems in iot based on autoencoder: A review," in *International Conference on Reliable Information and Communication Technology*. Springer, 2023, pp. 224–239.

[16] I. E. A. (IEA), "Canada 2022: Energy policy review," 2022, accessed: 2025-09-28. [Online]. Available: <https://www.iea.org/reports/canada-2022>

[17] S. Canada, "Energy use and greenhouse gas emissions in canada, 2022," 2022, accessed: 2025-09-28. [Online]. Available: <https://www15.statcan.gc.ca/n1/daily-quotidien/230627/dq230627c-eng.htm>

[18] United Nations, "The 17 sustainable development goals," <https://sdgs.un.org/goals>, 2025.

[19] N. Borgioli, F. Aromolo, L. T. X. Phan, and G. Buttazzo, "A convolutional autoencoder architecture for robust network intrusion detection in embedded systems," *Journal of Systems Architecture*, vol. 156, p. 103283, 2024.

[20] M. I. Beg and M. Y. Ansari, "Network intrusion detection system using autoencoders," in *2024 International Conference on Communication, Control, and Intelligent Systems (CCIS)*. IEEE, 2024, pp. 1–5.

[21] Y. S. Yap and M. R. Ahmad, "Modified overcomplete autoencoder for anomaly detection based on tinyml," *IEEE Sensors Letters*, vol. 8, no. 10, pp. 1–4, 2024.

[22] P. Vasiljevic, M. Matic, and M. Popovic, "Federated isolation forest for efficient anomaly detection on edge iot systems," *arXiv preprint arXiv:2506.05138*, 2025.

[23] J. Li, X. Zhang, H. Xiang, and A. Beheshti, "Federated anomaly detection with isolation forest for iot network traffics," in *2023 IEEE 29th International Conference on Parallel and Distributed Systems (ICPADS)*. IEEE, 2023, pp. 2622–2629.

[24] N. Li, X. Liu, Z. Liu, L. Mao, L. Zhao, and X. Wang, "Anomaly detection in power grid iot system based on isolated forest," in *IEEE/WIC/ACM International Conference on Web Intelligence and Intelligent Agent Technology*, 2021, pp. 9–12.

[25] W. Chen, "Anomaly detection method of new energy vehicle battery based on isolated forest algorithm," in *2024 5th International Conference for Emerging Technology (INCEET)*. IEEE, 2024, pp. 1–5.

[26] X. Cheng, Z. Liu, M. Tang, Y. Du, and C. Xu, "Anomaly detection based on improved isolated forest," in *2023 IEEE 3rd International Conference on Information Technology, Big Data and Artificial Intelligence (ICIBA)*, vol. 3. IEEE, 2023, pp. 971–975.

[27] J. Yang, X. Yang, and Z. Zhang, "A high-dimensional anomaly detection algorithm based on iforest with autoencoder," in *2022 4th International Conference on Data-driven Optimization of Complex Systems (DOCS)*. IEEE, 2022, pp. 1–5.

[28] X. Hu, Z. Zhang, R. Wang, and C. Hu, "Anomaly identification and prediction method for network timing data based on improved isolated forest approach," in *2025 IEEE 6th International Seminar on Artificial Intelligence, Networking and Information Technology (AINIT)*. IEEE, 2025, pp. 1–5.

[29] Y. Zhou, J. Cui, and Q. Liu, "Research and improvement of intrusion detection based on isolated forest and fp-growth," in *2020 IEEE 8th International Conference on Computer Science and Network Technology (ICCSNT)*. IEEE, 2020, pp. 160–164.

[30] B. Sharmila and R. Nagapadma, "Quantized autoencoder (qae) intrusion detection system for anomaly detection in resource-constrained iot devices using rt-iot2022 dataset," *Cybersecurity*, vol. 6, no. 1, p. 41, 2023.

[31] F. T. Liu, K. M. Ting, and Z.-H. Zhou, "Isolation forest," in *2008 eighth ieee international conference on data mining*. IEEE, 2008, pp. 413–422.

[32] M. Yousefi-Azar, V. Varadharajan, L. Hamey, and U. Tupakula, "Autoencoder-based feature learning for cyber security applications," in *2017 International joint conference on neural networks (IJCNN)*. IEEE, 2017, pp. 3854–3861.

[33] B. Briscoe, A. Brunstrom, A. Petlund, D. Hayes, D. Ros, J. Tsang, S. Gjessing, G. Fairhurst, C. Griwodz, and M. Welzl, "Reducing internet latency: A survey of techniques and their merits," *IEEE Communications Surveys & Tutorials*, vol. 18, no. 3, pp. 2149–2196, 2014.

[34] M. V. Devarakonda and R. K. Iyer, "Predictability of process resource usage: A measurement-based study on unix," *IEEE transactions on Software Engineering*, vol. 15, no. 12, pp. 1579–1586, 2002.

[35] A. Aloseel, S. Al-Rubaye, A. Zolotas, and C. Shaw, "Attack-detection architectural framework based on anomalous patterns of system performance and resource utilization—part ii," *IEEE Access*, vol. 9, pp. 87 611–87 629, 2021.

[36] A. M. Omer, "Energy use and environmental impacts: A general review," *Journal of renewable and Sustainable Energy*, vol. 1, no. 5, p. 053101, 2009.

[37] F.-J. Alvarado-Alcon, R. Asorey-Cacheda, A.-J. Garcia-Sanchez, and J. Garcia-Haro, "Carbon footprint vs energy optimization in iot network deployments," *IEEE Access*, vol. 10, pp. 111 297–111 309, 2022.

[38] Environment and Climate Change Canada. (2024, May) Emission factors and reference values, version 2.0. [Online]. Available: <https://www.canada.ca/en/environment-climate-change/services/climate-change/pricing-pollution-how-it-will-work/output-based-pricing-system/federal-greenhouse-gas-offset-system/emission-factors-reference-values.html>

[39] L. St, S. Wold *et al.*, "Analysis of variance (anova)," *Chemometrics and intelligent laboratory systems*, vol. 6, no. 4, pp. 259–272, 1989.

[40] C. E. Agbangba, E. S. Aide, H. Honfo, and R. G. Kakai, "On the use of post-hoc tests in environmental and biological sciences: A critical review," *Heliyon*, vol. 10, no. 3, 2024.

[41] N. A. Ahad and S. S. S. Yahaya, "Sensitivity analysis of welch's t-test," in *AIP Conference proceedings*, vol. 1605, no. 1. American Institute of Physics, 2014, pp. 888–893.

[42] G. H. Golub, A. Hoffman, and G. W. Stewart, "A generalization of the eckart-young-mirsky matrix approximation theorem," *Linear Algebra and its applications*, vol. 88, pp. 317–327, 1987.

[43] T. Van Erven and P. Harremos, "Rényi divergence and kullback-leibler divergence," *IEEE Transactions on Information Theory*, vol. 60, no. 7, pp. 3797–3820, 2014.

[44] T. Rhodes and D. Lee, "Local disentanglement in variational auto-encoders using jacobian l_1 regularization," *Advances in Neural Information Processing Systems*, vol. 34, pp. 22 708–22 719, 2021.

[45] V. Venkateswaran, "Bot_iot dataset," <https://www.kaggle.com/datasets/vigneshvenkateswaran/bot-iot>, 2020.

[46] B. H. Ali, N. Sulaiman, S. Al-Haddad, R. Atan, and S. L. M. Hassan, "Ddos detection using active and idle features of revised cicflowmeter and statistical approaches," in *2022 4th International Conference on Advanced Science and Engineering (ICOASE)*. IEEE, 2022, pp. 148–153.

[47] M. A. Khan, A. Azim, R. Liscano, K. Smith, Y.-K. Chang, G. Seferi, and Q. Tauseef, "On the effectiveness of feature selection techniques in the context of ml-based regression test prioritization," *IEEE Access*, 2024.

[48] J. M. Adeke, G. Liu, L. Amoah, and O. J. Nwali, "Investigating the impact of feature selection on adversarial transferability in intrusion detection system," *Computers & Security*, vol. 151, p. 104327, 2025.

[49] S. B. Alias, S. Manickam, and M. M. Kadhum, "A study on packet capture mechanisms in real time network traffic," in *2013 International Conference on Advanced Computer Science Applications and Technologies*. IEEE, 2013, pp. 456–460.

[50] D. Stiawan, D. Wahyudi, T. W. Septian, M. Y. Idris, and R. Budiarso, "The development of an internet of things (iot) network traffic dataset with simulated attack data," *Journal of Internet Technology*, vol. 24, no. 2, pp. 345–356, 2023.

- [51] A. Pasquini, R. Vasa, I. Logothetis, H. H. Gharakheili, A. Chambers, and M. Tran, "Descriptor: Deakin iot traffic (d-iot)," *IEEE Data Descriptions*, 2025.
- [52] A. Chatterjee and B. S. Ahmed, "Iot anomaly detection methods and applications: A survey," *Internet of Things*, vol. 19, p. 100568, 2022.
- [53] R. Singh and S. S. Gill, "Edge ai: a survey," *Internet of Things and Cyber-Physical Systems*, vol. 3, pp. 71–92, 2023.
- [54] S. Heydari and Q. H. Mahmoud, "Tiny machine learning and on-device inference: A survey of applications, challenges, and future directions," *Sensors*, vol. 25, no. 10, p. 3191, 2025.
- [55] R. Das and T. Luo, "Lightesd: Fully-automated and lightweight anomaly detection framework for edge computing," in *2023 IEEE International Conference on Edge Computing and Communications (EDGE)*. IEEE, 2023, pp. 150–158.
- [56] P. Madadi, F. Baccelli, and G. de Veciana, "Shared rate process for mobile users in poisson networks and applications," *IEEE Transactions on Information Theory*, vol. 64, no. 3, pp. 2121–2141, 2017.
- [57] C. Wohlin, P. Runeson, M. Höst, M. C. Ohlsson, B. Regnell, and A. Wesslén, *Experimentation in software engineering*. Springer Science & Business Media, 2012.

XI. EXTENDED MATHEMATICAL DERIVATIONS FOR ECODEFENDER

This appendix provides extended mathematical formulations underlying the *EcoDefender* framework. The derivations formalize the normalization process, latent regularization, and manifold alignment mechanisms used in the AE-IF hybrid model. Additionally, we present analytical expressions for energy-latency coupling, dynamic resource optimization, and adversarial robustness, illustrating how these components collectively govern performance, efficiency, and sustainability at the network edge.

A. Normalized Data Transformations

To ensure stable feature scaling and robustness against outliers, input features are normalized using a composite of z-score, log, and IQR-based transformations:

$$x'_{ij} = \frac{x_{ij} - \mu_j}{\sigma_j + \epsilon} + \delta_1 \log\left(1 + \frac{|x_{ij} - \mu_j|}{\sigma_j}\right) + \delta_2 \frac{x_{ij} - \text{median}(x_j)}{IQR(x_j)}, \quad (70)$$

$$\bar{x}_j = \frac{1}{N} \sum_i x'_{ij}, \quad \tilde{x}_j = \frac{x'_{ij} - \bar{x}_j}{\sqrt{\frac{1}{N} \sum_i (x'_{ij} - \bar{x}_j)^2}}. \quad (71)$$

B. Latent Space Regularization

The encoder compresses the input to latent vectors, while regularization enforces smoothness and stability in the learned manifold:

$$z_i = f_{enc}(x_i) = \sigma(W_{enc}x_i + b_{enc}), \quad (72)$$

$$\hat{x}_i = f_{dec}(z_i) = \sigma(W_{dec}z_i + b_{dec}), \quad (73)$$

$$\mathcal{R}_s = \|x_i - \hat{x}_i\|_2^2 + \lambda_1 \text{Tr}(W_{enc}^\top W_{enc}) + \lambda_2 \|z_i\|_2^2, \quad (74)$$

$$\nabla_{W_{enc}} \mathcal{R}_s = 2(W_{enc}W_{enc}^\top - I)W_{enc}. \quad (75)$$

C. Manifold Alignment Term

This term aligns encoder and decoder subspaces to preserve geometric consistency:

$$\mathcal{L}_{align} = \gamma \tanh(\text{Tr}(W_{enc}^\top W_{dec})) + \eta \|W_{enc}W_{dec}^\top - I\|_F^2, \quad (76)$$

$$\frac{\partial \mathcal{L}_{align}}{\partial W_{enc}} = \gamma W_{dec} \text{sech}^2(\text{Tr}(W_{enc}^\top W_{dec})) + 4\eta(W_{enc}W_{dec}^\top - I)W_{dec}^\top. \quad (77)$$

D. Composite Optimization Function

The global training objective integrates reconstruction, regularization, and manifold consistency terms:

$$\begin{aligned} \mathcal{J}_{AE-IF} = & \frac{1}{N} \sum_{i=1}^N \left[\|x_i - \hat{x}_i\|_2^2 + \beta D_{KL}(p(z_i) \| \mathcal{N}(0, I)) \right. \\ & + \lambda_1 \|J_{f_{enc}}(x_i)\|_F^2 + \lambda_2 \mathbb{E}_{\mathcal{T}}[h(x_i, \mathcal{T})] \\ & \left. + \lambda_3 \|W_{enc}\|_F^2 + \lambda_4 \|W_{dec}\|_F^2 + \xi \mathcal{L}_{align} \right]. \quad (78) \end{aligned}$$

E. Energy and Latency Coupling

Energy models capture computational and structural dependencies between encoder and forest components:

$$E_{AE} = \kappa_{AE}(NdL) + \xi_1 \sum_{i=1}^L \|W_i\|_F^2, \quad (79)$$

$$E_{IF} = \kappa_{IF}(mn \log n) + \xi_2 m h_{avg}, \quad (80)$$

$$E_{total} = E_{AE} + E_{IF} + \xi_3 \|Z\|_2^2, \quad (81)$$

$$T_{latency} = \frac{\partial E_{total}}{\partial f_{cpu}} + \frac{\partial E_{total}}{\partial M_{cache}} + \frac{\partial E_{total}}{\partial B_{net}}. \quad (82)$$

F. Dynamic Resource Allocation

Optimal resource configuration is determined through multi-objective optimization that balances performance and energy:

$$R_{opt} = \arg \min_{r \in \mathcal{R}} (E_{total}(r) - \lambda_P P_{acc}(r)), \quad (83)$$

$$\frac{\partial E_{total}}{\partial r} = \lambda_P \frac{\partial P_{acc}}{\partial r}, \quad (84)$$

$$r^* = \frac{\lambda_P}{\lambda_E} \frac{dP_{acc}}{dE_{total}}. \quad (85)$$

G. Adversarial Robustness Margin

Robustness is characterized as the minimum perturbation that alters the joint reconstruction score output:

$$R(x) = \min_{\|\delta\|_p < \epsilon} (e(x + \delta) + s(x + \delta)), \quad (86)$$

$$\delta^* = -\epsilon \frac{\nabla_x(e(x) + s(x))}{\|\nabla_x(e(x) + s(x))\|_p}, \quad (87)$$

$$R^*(x) = e(x + \delta^*) + s(x + \delta^*). \quad (88)$$

H. Information-Theoretic Robustness

The mutual information between inputs and latent representations quantifies embedding stability:

$$I(x; z) = H(z) - H(z|x), \quad (89)$$

$$H(z) = - \int p(z) \log p(z) dz, \quad (90)$$

$$I(x; z) \leq \frac{1}{2} \log \det(I + \Sigma_x W_{enc}^\top W_{enc}), \quad (91)$$

$$\nabla_{W_{enc}} I(x; z) = (\Sigma_x W_{enc})(I + \Sigma_x W_{enc}^\top W_{enc})^{-1}. \quad (92)$$

Hybrid Statistical Decision Boundary

The optimal decision threshold is derived from the intersection of Gaussian likelihoods:

$$\begin{aligned} P(F(x) > \tau | y = 0) &= \int_{\tau}^{\infty} \frac{1}{\sqrt{2\pi\sigma_0^2}} e^{-\frac{(F-\mu_0)^2}{2\sigma_0^2}} dF, \\ \frac{dP_e}{d\tau} &= \frac{\pi_0(\tau - \mu_0)}{\sigma_0^2} e^{-\frac{(\tau-\mu_0)^2}{2\sigma_0^2}} - \frac{\pi_1(\mu_1 - \tau)}{\sigma_1^2} e^{-\frac{(\mu_1-\tau)^2}{2\sigma_1^2}}, \quad (93) \end{aligned}$$

$$\tau^* = \frac{\mu_0\sigma_1^2 - \mu_1\sigma_0^2 + \sigma_0\sigma_1 \sqrt{(\mu_1 - \mu_0)^2 + 2(\sigma_1^2 - \sigma_0^2) \ln \frac{\pi_1\sigma_1}{\pi_0\sigma_0}}}{\sigma_1^2 - \sigma_0^2}. \quad (94)$$

J. Spectral Analysis of Weight Matrices

Spectral norms control stability and prevent weight explosion:

$$\lambda_{\max}(W_{enc}) \leq \|W_{enc}\|_2 \leq \sqrt{\text{Tr}(W_{enc}^\top W_{enc})}, \quad (95)$$

$$\text{cond}(W_{enc}) = \frac{\lambda_{\max}(W_{enc})}{\lambda_{\min}(W_{enc})}, \quad (96)$$

$$\mathcal{R}_{spec} = \sum_i \left(\frac{\lambda_i(W_{enc})}{\bar{\lambda}} \right)^2 + \sum_j \left(\frac{\lambda_j(W_{dec})}{\bar{\lambda}} \right)^2. \quad (97)$$

K. Energy–Accuracy Pareto Frontier

The trade-off between accuracy and energy defines the Pareto frontier for sustainable optimization:

$$\frac{\partial \mathcal{A}}{\partial E} = \frac{\nabla_{\theta} \mathcal{A}}{\nabla_{\theta} E}, \quad (98)$$

$$\mathcal{A}(E) = \mathcal{A}_0 + \int_{E_0}^E \frac{\nabla_{\theta} \mathcal{A}}{\nabla_{\theta} E} dE, \quad (99)$$

$$\mathcal{A}_{opt} = \max_E (\mathcal{A}(E) - \lambda_E E). \quad (100)$$